1989

Two-Dimensional ^{1}H and ^{31}P NMR Spectra of a Decamer Oligodeoxyribonucleotide Duplex and a Quinoxaline ([MeCys^{3}, MeCys^{7}]TANDEM) Drug Duplex Complex

Robert Powers
University of Nebraska - Lincoln, rpowers3@unl.edu

Richard K. Olsen
Utah State University

David G. Gorenstein
Purdue University

Published in *Journal of Biomolecular Structure and Dynamics* 7:3 (1989), pp. 515–556;
doi: 10.1080/07391102.1989.10508507.

Submitted July 10, 1989.

Two-Dimensional ^{1}H and ^{31}P NMR Spectra of a Decamer Oligodeoxyribonucleotide Duplex and a Quinoxaline ([MeCys^{3}, MeCys^{7}]TANDEM) Drug Duplex Complex

Robert Powers,[1] Richard K. Olsen,[2] and David G. Gorenstein[1]

1. Department of Chemistry, Purdue University, West Lafayette, Indiana 47907
2. Department of Chemistry, Utah State University, Logan, Utah 84322

Abstract

Assignment of the ^{1}H and ^{31}P NMR spectra of a decamer oligodeoxyribonucleotide duplex, d(CCCGATCGGG), and its quinoxaline ([MeCys^{3}, MeCys^{7}]TANDEM) drug duplex complex has been made by two-dimensional ^{1}H-^{1}H and heteronuclear ^{31}P-^{1}H correlated spectroscopy. The ^{31}P chemical shifts of this 10 base pair oligonucleotide follow the general observation that the more internal the phosphate is located within the oligonucleotide sequence, the more upfield the ^{31}P resonance occurs. While the ^{31}P chemical shifts show sequence-specific variations, they also do not generally follow the Calladine "rules" previously demonstrated. ^{31}P NMR also provides a convenient monitor of the phosphate ester backbone conformational changes upon binding of the drug to the duplex. Although the quinoxaline drug, [MeCys^{3}, MeCys^{7}]TANDEM, is generally expected to bind to duplex DNA by bis-intercalation, only small ^{31}P chemical shift changes are observed upon binding the drug to duplex d(CCCGATCGGG). Additionally, only small perturbations in the ^{1}H NMR and UV spectra are observed upon binding the drug to the decamer, although association of the drug stabilizes the duplex form relative to the other states. These results are consistent with a nonintercalative mode of association of the drug. Modeling and molecular mechanics energy minimization demonstrate that a novel structure in which the two quinoxaline rings of the drug binds in the minor groove of the duplex is possible.

Introduction

It is now widely appreciated that duplex DNA can exist in a number of different conformations (1). Significant conformational differences can exist globally along the entire double helix, as in the A, B, C, and Z forms of DNA (1). In addition, local conformational heterogeneity in the deoxyribose phosphate backbone has been most recently noted in the form of sequence-specific variations (2–4) or as the result of drug (1) or protein binding (5,6) to local regions of the DNA. While X-ray crystallography has provided much of our understanding of these DNA structural variations, increasingly, high resolution NMR has also begun to provide detailed three-dimensional structural information on duplex oligonucleotides (7–16) and drug duplex complexes.

Bis-intercalators

There is a limited amount of structural information on the bis-intercalators–DNA binding drugs that possess two covalently linked intercalating rings. Studies have centered primarily around acridine dimers, ethidium dimers, ditercalinium, and more recently echinomycin, triostin A, and their derivatives (17–24). The latter two are members of the quinoxaline class of naturally occurring antibiotic, antimicrobial, and antitumor drugs (25–27). Quinoxalines are divided into two subclasses: quinomycins (such as echinomycin) and the triostins, which are differentiated by the type of sulfur bonds across the cyclic depsipeptide (fig. 1). The triostins have a simple disulphide bridge while the quinomycins have a thioacetal cross-bridge.

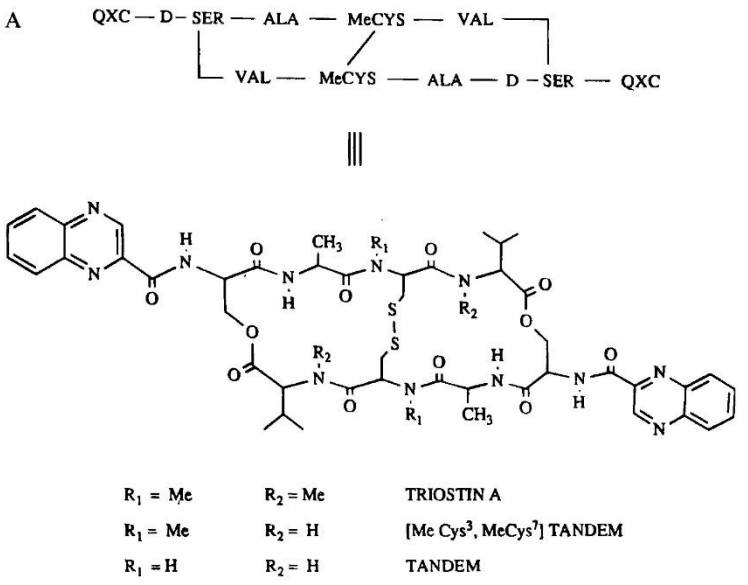

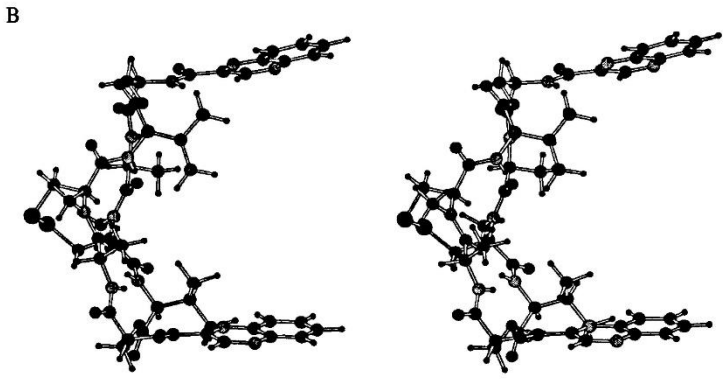

Figure 1. (A) Structures of bis-intercalators, Trisotin A, [MeCys^3, MeCys^7]TANDEM, and TANDEM. (B) Stereo view of [MeCys^3, MeCys^7]TANDEM based upon the X-ray structure of TANDEM.

They are C-shaped (fig. 1B) with a pair of parallel quinoxaline rings perpendicular to the cyclic depsipeptide (28–31).

The initial interest in bis-intercalators was in designing drugs with higher DNA binding affinity and sequence specificity. The rationale behind this research was the existence of a good correlation between DNA binding affinity and the drug's efficacy against L 1210 murine leukemia in female DBA/2 mice and the growth of P-388 cells in culture and in DBA/2 mice (32,33). The bis-intercalators with a higher DNA binding affinity demonstrated a higher antitumor activity. The effect of bis-intercalation was also examined by the ability

of these compounds to inhibit *E. coli* DNA polymerase I (21). Bis-intercalating compounds inhibited this process more efficiently than did the corresponding mono-intercalators.

The identification of the bis-intercalation mode of binding was based primarily on their ability to unwind closed circular DNA and lengthen the DNA helix. This process was monitored by the change in the sedimentation coefficient and viscosity of the DNA with the addition of drug. The results were referenced to the ethidium monomer which is a known mono-intercalator with a defined unwinding angle of 26°. All of the studied drugs demonstrated a relative unwinding angle of approximately twice that of the ethidium monomer (17,18,26,27,34). In addition to viscometric studies, electron microscopy was used to measure the lengthening of the DNA helix by the presence of the drug (20). All of the bis-intercalators lengthened the DNA helix approximately twice the distance of ethidium bromide at the same drug/base-pair ratio. The presence of intercalation was also monitored by the typical bathochromic and hypochromic shifts of UV spectra for intercalators (26,35). More recently, an X-ray crystal structure of a triostin A–d(CGTACG)$_2$ complex clearly shows both quinoxaline chromophores intercalated between the GC base pairs with the cyclic depsipeptide situated in the minor groove forming hydrogen bonds between the alanine residues NH and the guanosine N-3 (36). NMR studies of ethidium dimer–poly(dA-dT)$_2$, diacridines-d(AT)$_5$-d(AT)$_5$, diacridine-d(CGCG)$_2$, and diacridine–calf thymus DNA and echinomycin-d(ACGT)$_2$ complexes have supported the bis-intercalation of these drugs by observing upfield shifts of imino, and aromatic protons affected by the nuclear shielding of the stacked chromophore and observing drug-DNA NMR data consistent with bis-intercalation. In particular, nuclear Overhauser effects were observed between the ditercalinium's chromophore protons and the H1′, H2″, and base protons of the GC base pair in the ditercalinium-d(CGCG)$_2$ complex (23) as well as a fairly complete set of intermolecular NOEs establishing the solution structure of an echinomycin-d(ACGT)$_2$ complex (24). The later study represents the only NMR study on the DNA binding of the quinoxaline family of bis-intercalators. The present study deals with the analysis of a triostin A analog ([MeCys^3, MeCys^7]TANDEM) binding to the duplex decamer d(CCCGATCGGG)$_2$. The study involves UV, ^{31}P, and ^{1}H NMR analysis of the [MeCys^3, MeCys^7]TANDEM · d(CCCGATCGGG)$_2$ drug duplex complex. The results indicate that the binding of [MeCys^3, MeCys^7]TANDEM to the decamer is not by intercalation but appears to bind in a nonspecific manner to the minor groove of the DNA.

Experimental Methods

Materials

The self-complementary decamer d(CCCGATCGGG) was synthesized by a manual modification of the solid phase phosphite triester method (using 10 μmole of the starting nucleoside derivatized support) as previously described (12,37–39). The purity of the decamer was verified by chromatography on an anion-exchange column, a silica column coated with crosslinked polyethylene imine (40). The decamer NMR sample was prepared by dissolving ca. 500 OD units in 0.4 ml 100 mM phosphate buffer (D_20) pH 7.0 (uncorrected pH meter reading), 100 mM KCl, 1 mM EDTA, 1 mM sodium azide.

The decamer was labeled with ^{17}O and ^{18}O to assist in the assignment of the ^{31}P spectrum. The $^{17}O/^{18}O$ label was incorporated at the appropriate step in the DNA sequence by using $^{17}O/^{18}O$ water during the oxidation step of the DNA synthesis as previously described (12,37).

The [MeCys³, MeCys⁷]TANDEM sample was prepared as previously described (41,42).

A decamer · [MeCys³, MeCys⁷]TANDEM (0.8:1) complex was made by adding 6.94 mg (12 μmol) [MeCys³, MeCys⁷]TANDEM to a 8.25 μmol sample of decamer in ca. 1 mL of water. Approximately 20% acetonitrile was added to the mixture to bring [MeCys³, MeCys⁷]TANDEM into solution. The sample was shaken vigorously for 24 hours, followed by centrifugation to remove undissolved drug and the supernatant roto-evaporated to remove most of the acetonitrile. The sample was then repeatedly dissolved in double distilled water, centrifuged, and the supernatant lyophilized to remove the remaining acetonitrile. A small amount of acetonitrile remained in the golden orange color solution. The sample was treated with Chelex-100 resin again for the NMR studies (the UV spectrum did not change upon Chelex treatment). The concentration of decamer and duplex in solution for both the UV (see below) and NMR studies was estimated from the UV spectrum of the drug complex utilizing the extinction coefficients of the duplex and drug measured separately. They were consistent with an ca. 0.8:1 ratio of drug/duplex (estimated error ± 10%).

UV spectra were collected on a CARY 210 UV spectrophotometer with a temperature-controlled sample holder. A 1 cm pathlength cell was used for the UV spectra. All UV samples were a 1,000 fold dilution of the corresponding NMR sample, resulting in an OD of approximately 0.5 at λ_{max} of 260 nm. The decamer and decamer · [MeCys³, MeCys⁷]TANDEM samples were aqueous solutions with a KCl concentration of 100 mM and 100 mM phosphate buffer pH 7.0. The decamer UV melting curves were measured at two concentrations (6.0 and 3.0 μM) and a range of salt concentrations (0–400 mM KCl). For the UV titration study, the 1 ml decamer · [MeCys³, MeCys⁷]TANDEM complex was titrated with 0.13 O.D. 1 μl aliquots of decamer. The resulting spectra were observed against either a blank solution or the decamer · [MeCys³, MeCys⁷]TANDEM.

NMR spectra of the decamer and decamer · [MeCys³, MeCys⁷]TANDEM samples were performed on either a Nicolet NTC-470, 470 MHz NMR instrument or a Varian XL-200A, 200 MHz NMR spectrometer. The ^1H NMR spectra, the 2D NOESY and COSY spectra for both the decamer and decamer · [MeCys³, MeCys⁷]TANDEM samples were run on the Nicolet NTC-470. The ^1H spectra were referenced to H_20 at 4.76 ppm. A spectral window of 5000 Hz was used for all the NTC-470 experiments except for the temperature dependence of the imino protons in which a spectral window of 10000 Hz was used. For the one-dimensional experiments, 8K data points were collected. For the two-dimensional experiments 256 FIDs by 2K data sets were collected. The HDO solvent signal was saturated with a decoupler pulse of 55 dB and pulse width of 30 μs. In addition, a noise generator centered at the water resonance was used for all ^1H NMR experiments except for the imino melting profile experiments. The decoupler pulse was off during acquisition.

The ^{31}P ID NMR spectra, the ^{31}P melting profiles, the $^1H/^{31}P$ correlation COLOC (PAC) spectra, and the $^1H/^{31}P$ heteronuclear 2D J-resolved spectrum were run on the XL-200A. All experiments were run in either 99.998% D_2O or 85%H_2O/15%D_2O. Typical ^{31}P 1D NMR parameters were as follows: sweep width 172 Hz; acquisition time 2.98 s; block size 1K

zero filled to 16K; pulse width 7.0 μs; spectra were resolution enhanced with a combination of positive exponential and Gaussian apodization functions; the number of acquisitions was between 2000 and 3000. The ^{31}P spectra were referenced to trimethyl phosphate (TMP) at 0.000 ppm, which is 3.456 ppm downfield of 85% phosphoric acid.

The temperature dependence of the imino proton ^{1}H spectrum was measured with a modified one-dimensional water suppression sequence (WS1D; 43). The WS1D sequence is:

RD-HSP-90-D-90-HSP-90-D-D-90-HSP-acq

where:

RD = recovery delay
HSP = homospoil pulse and recovery
D = delay optimized for imino protons.

The water suppression technique employs a spin-echo sequence to specifically subtract out the HDO resonance. The above sequence contains four phase-cycled 90° pulses separated by either a homospoil pulse along the *z* and *y* axis or a delay optimized for the resonances of interest, which will rotate by 90° or 270° relative to the stationary HDO resonance.

The 90° pulse used was dependent on temperature and ranged from 20 μs to 32 μs. The homospoil pulse was 2.0 ms with a recovery period of 200 μs. A delay of 180 μs corresponded to the difference in the imino and HDO resonances. A 2.0 s recovery delay was used and the experiment was run with the sample nonspinning. Spectra were recorded from 5 to 50°C at 5° intervals based on the NTC-470 thermocouple reading. Temperatures were calibrated by using a methanol thermometer for temperatures up to 40°C.

The ^{1}H chemical shifts were referenced to the 4.76 ppm HDO signal. All imino peak integrations were referenced to the most downfield proton at 50°C, which was set to a value of one proton. The decamer sample was run at both a 100 mM and 400 mM KCl concentrations.

Absolute value $^{1}H/^{1}H$ COSY was taken of the decamer sample. The pure-absorption phase COSY spectra of the drug-duplex complex were acquired. The spectra were acquired with a sweep width of 5000 Hz. Approximately 320 transients were taken for each of the 256 FIDs with 2K data points of resolution. A 90° pulse of 14.6–15 μs and a recycle delay of 2.2 s (absolute value spectra) or 3.5 s (pure absorption phase spectra) were used. For both experiments, the initial t_1 value was 100 μs and it was increased by 100 μs intervals. The data was processed with 2K of zero filling in both the t_1 and t_2 dimension. A skewed sign bell apodization function was used in the t_2 dimension. The t_1 dimension was processed with either magnitude calculation and an exponential apodization function with line broadening of 10 Hz for the absolute value spectra or a skewed sign bell apodization function for the pure absorption phase spectra.

Two-dimensional NOESY were acquired in the phase-sensitive mode using the TPPI (44) phase-cycling scheme. The spectra were acquired with 2048 points in the t_2 (acquisition) dimension with 1024 t_1 increments. The mixing times (τ_m) ranged from 50 to 700 ms for the decamer sample (200 and 400 ms mixing times were used for the decamer · [MeCys^3,

MeCys^7]TANDEM complex). The recovery delay time for the decamer was 2.2 s. 90° pulses ranged from 11–14 μs for the decamer sample. The recovery delay for the decamer · [MeCys^3, MeCys^7]TANDEM sample was 2.2 s for 200 ms mixing time and 3.5 s for 400 ms mixing time. 90° pulses ranged from 14–15 μs for the decamer · [MeCys^3, N-MeCys^7]TANDEM sample. The experiment was run with the sample nonspinning to minimize t_1 noise. For spectra recorded in 85%H_2O/15%D_2O, the H_2O signal was irradiated during the mixing time and the delay between scans. A homospoil pulse of 20 ms with a recovery time of 20 ms was applied just prior to the first 90° pulse.

The resulting data was processed using Dennis Hare's FTNMR program, V4.5 or V4.7. The data was processed with zero filling to 2K in both t_2 and t_1 dimensions. An exponential line broadening of 1 Hz was used to apodize the data in the t_2 dimension. A trapezoidal apodization function was used for all the TPPI NOESY mixing times when the crosspeak volumes were measured using the FTNMR program. The 400 ms TPPI NOESY was apodized with a Gaussian multiplication in both t_1 and t_2 dimension when the resulting spectrum was used strictly for the assignment of the proton spectrum.

The NOE crosspeak volumes were measured with FTNMR. The volumes were measured with either a constant J value of 1 or one optimized by the program (V4.7), ranging from 1 to 3 depending on the size of the NOE crosspeak. The J value defined the width of the ellipse used to approximate the crosspeak. The calculated distances utilizing either approaches were similar.

Although volumes were measured for a complete set of mixing times (50–700 ms) the volumes for a single 200 ms TPPI NOESY were used to measure the intra and inter proton distances from the observed NOE crosspeaks. The internal ruler for measuring the distances from the observed volumes was the H5-H6 NOE of C3. This resolved NOE was assigned a value of 2.45 Å. The volume of a crosspeak, and its corresponding distance, was not measured if a significant amount of crosspeak overlap existed.

A $^{31}P/^1H$ *P*ure *A*bsorption Phase *C*onstant Time (PAC) version of the Kessler-Griesinger Long-Range Heteronuclear Correlation (COLOC) experiment (45) was conducted on the decamer and the decamer · [MeCys^3, MeCys^7]TANDEM complex (46,47). The preacquisition delay was 2 s, the constant delay was 0.051 s, and the refocusing delay was 0.035 s. A first order phase correction of 12,075° was used in the ω_1 dimension. The PAC spectra were acquired with a sweep width of 122.8 Hz in the t_2 dimension and 641.9 Hz in the t_1 dimension. The experiments were collected with 400–600 transients for each of the 64 FIDs with 256 data points of resolution. A 90° pulse of 7.5 μs for phosphorus and 80 μs for protons was used. The data was processed with 1K zero filling in the t_1 dimension and 512 zero filling in the t_2 dimension. A Gaussian apodization was applied in both the t_1 and t_2 dimension to give resolution enhancement.

The Bax-Freeman Selective 2D-J Resolved Long-Range Correlation experiment with a Dante sequence for the selective 180° pulse (48) was performed on the decamer and the decamer-TANDEM complex to correlate the ^{31}P chemical shift with the phosphorus-H3′ coupling constant. A Dante pulse chain consisted of 20 pulses of an approximate length of 9° (total of 180°). The 9° pulse (8 μs) consisted of 0.4 μs of dead time. In addition, the pulses were separated by a delay of 2 μs. The selective 2D-J long-range correlation experiment was acquired with a sweep width of 50 Hz in the t_1 dimension and 503.6 Hz in the t_2 dimension.

A 90° phosphorus pulse width of 7.5 μs and a 8.8 μs proton pulse width and a recycle delay of 1.5 s was used. The experiment was collected with 1100–1600 transients for each of the 32 FIDs with 448 data points in t_1. A t_1 value of 0.l s was used. The data was processed with 1K zero filling in both the t_2 and t_1 dimension with a Gaussian apodization function to give resolution enhancement in both dimensions.

The observed three-bond coupling constant is used with a proton-phosphorus Karplus relationship to measure the H3′-C3′-O-P torsional angle θ from which we have calculated the C4′-C3′-O-P torsional angle ε (= θ – 240°). The equation $J = 15.3\cos^2(\theta) - 6.1\cos(\theta) + 1.6$ was used (48,49).

The 1D^{31}P spectra were collected with a sweep width of 1000 Hz, 2Kdata points with 16K zero filling. A 90° pulse width of 7.5 μs, recycle delay of 1 s and either 256 or 512 transients were used to collect the spectrum. The data was processed with a Gaussian apodization function to give resolution enhancement. The temperatures of the ^{1}H-decoupled ^{31}P NMR samples were corrected for decoupler heating of the sample. The ^{31}P "thermometer" consisted of a sample of phosphoric acid and trimethyl phosphate as previously described (50). Note that even with WALTZ decoupling we find that decoupler heating can raise the temperature of the sample by as much as 4°C.

NOESY Distance Constrained Molecular Mechanics Calculations of Duplex and Molecular Mechanics Calculations of Duplex · Drug Complex

The molecular mechanics/dynamics program AMBER (51) was used to initially generate an idealized Arnott B-DNA decamer duplex structure (52). NOESY distance constraints were incorporated into the AMBER potential energy function through addition of a flat well potential (see Results). The model-built structure with 122 NOESY distance constraints were then energy refined until a rms gradient of 0.l kcal/mol-Å was achieved or until the change in energy was less than 1.0×10^{-7} kcal/mol for successive steps.

The molecular mechanics program (AMBER) was also used to generate a molecular mechanics minimized structure for the decamer · [MeCys^3, MeCys^7]TANDEM complex. The decamer structure in the complex was based upon the NOE constrained and minimized structure of the free decamer. The [Met Cys^3, Met Cys^7] TANDEM structure was derived from the X-ray structure coordinates of TANDEM (28,29). The difference between TANDEM and [Met Cys^3, Met Cys^7]TANDEM is the N-methyl group on each of the L-cysteines. Charges for the serine quinoxaline and subfragment N-Met Cys of TANDEM were calculated using AM1 (53) with coordinates obtained from the X-ray structure of TANDEM. After both the decamer and [MeCys^3, MeCys^7]TANDEM were minimized with AMBER, [MeCys^3, MeCys^7]TANDEM was docked onto the NOESY distance-constrained, energy-minimized decamer duplex using MIDAS (54). After docking [MeCys^3, MeCys^7]TANDEM onto the decamer with MIDAS, the complex was energy minimized with the AMBER program.

Results

Assignments of ^{31}P Signals of Decamer Oligonucleotide Duplex

The ^{31}P spectrum for the decamer

dCCCGATCGGG
dGGGCTAGCCC
1

is shown in figure 2.

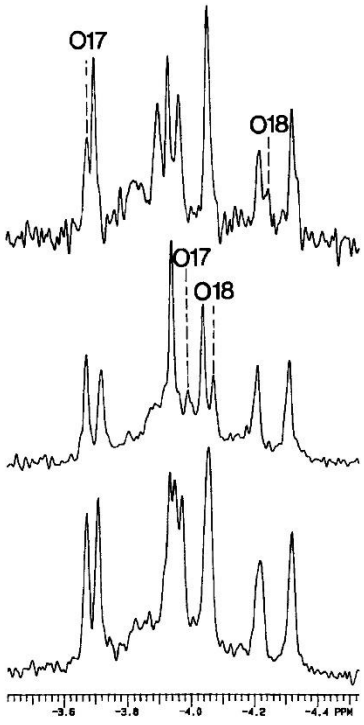

Figure 2. ^{31}P NMR spectra of decamer (bottom). Examples of site-specific ^{17}O and ^{18}O labeling of two of the phosphates of the decamer at positions C2pC3 (^{17}O) and G4pA5 (^{18}O) (middle) and at positions G8pG (^{17}O) and T6pC7 (^{18}O) (top) are shown.

The decamer's ^{31}P signals were assigned by both a 2D pure absorption phase constant time (PAC) heteronuclear correlation NMR (46,55) and ^{17}O/^{18}O labeling methodologies (12).

As shown in figure 3 the PAC spectrum contains a pair of crosspeaks between the phosphorus resonance and either an H3′/H4′ pair or an H3′/H5′ pair—the proton signals had been previously assigned by the 2D ^{1}H/^{1}H spectra (see below). Assignment of the ^{31}P signal of the ith phosphate was achieved through connectivities with both the 3′H(i) and 4′H (i + 1) or 5′H(i + l)/5″H(i + 1) deoxyribose protons (39,56). Although the 5′H(i + 1) and 5″H(i + 1)

protons overlap with the 4′ protons, the intensities for the ^{31}P-5′H and 5″H PAC crosspeaks generally appear to be weaker than the 4′H crosspeaks. These pairs of protons from the PAC spectrum were then matched to appropriate pairs from the TPPI NOESY spectrum to complete the assignment of the ^{31}P spectrum.

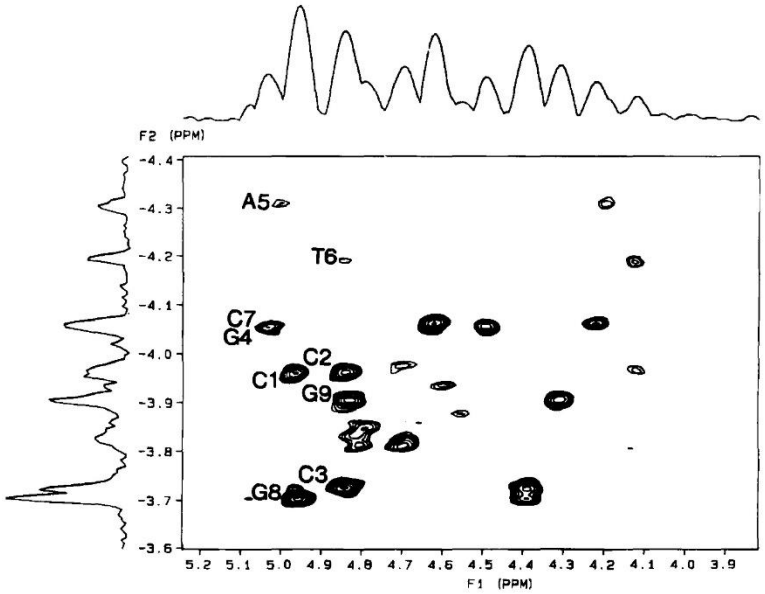

Figure 3. Two-dimensional ^{31}P-^{1}H PAC heteronuclear correlation NMR spectrum of duplex decamer at 200 MHz (^{1}H). The 1D decoupled ^{31}P NMR spectrum is shown along one axis and the H3′, H4′, and H5′5″ region of the proton spectrum is shown along the second axis.

There existed some ambiguities in the assignments because of the similarity in chemical shifts of a number of the H3′ protons and the ambiguities in the assignments of H4′, H5′, and H5″ in several of the residues. Surprisingly, we observe some crosspeaks to both H4′, H5′ and H5″ for several residues, in contrast to our earlier PAC spectra with a tetradecamer in which only 3′ and 4′ crosspeaks were observed (46). The assignments of the ^{31}P signals of some of the phosphates of the decamer *1* were verified by the ^{17}O/^{18}O labeling methodology. We can readily introduce both ^{17}O and ^{18}O labels into the phosphoryl groups by replacing the $I_2/H_2^{17}O$ in the oxidation step of the intermediate phosphite triester by $I_2/H_2^{17}O$ and $H_2^{18}0$ (12,37). In an earlier study on a tetramer oligonucleotide (37), our laboratory had demonstrated that all three phosphate signals could be assigned by synthesizing the oligonucleotide with ^{17}O, ^{18}O, and ^{16}O (unlabeled) in each of the three different phosphate positions. Later studies on longer oligonucleotides (12,15,57–63) relied on single, regiospecific ^{17}O labeling of the oligonucleotides, which, of course, requires separate n-1 syntheses for each of the n phosphate positions of the oligonucleotide and is thus more time consuming. By simultaneously incorporating a single mono-^{17}O phosphoryl and a separate mono-^{18}O phosphoryl labeled oligonucleotide (two specific phosphates are labeled along the

strand), we can simultaneously identify the ^{31}P signals of two phosphate diester signals (assuming we can resolve the effect of the ^{17}O and ^{18}O label on the ^{31}P signals). The quadrupolar ^{17}O nucleus (generally ca. 40% enriched) broadens the ^{31}P signal of the directly attached phosphorus to such an extent that only the high-resolution signal of the remaining 60% nonquadrupolar broadened phosphate at the labeled site is observed (37,59,61). Thus a decrease in intensity is observed for the phosphate signal labeled with ^{17}O.

We can also identify the phosphate diester attached to the ^{18}O label because of an isotope effect on the ^{31}P chemical shifts (37). The ^{18}O isotope affects the ^{31}P resonances by inducing a small upfield isotope shift of 0.01–0.02 ppm. Therefore, if resolution is good enough, the presence of the upfield isotope shifted peak in the ^{31}P spectrum indicates the ^{18}O labeled phosphorus.

In this way six different $^{17}O/^{18}O$ double labeled decamer samples with a different disubstituted $^{17}O/^{18}O$-phosphoryl group allows identification of two specific ^{31}P signal and the full series of dilabeled oligonucleotides gives the assignment of the entire ^{31}P NMR spectrum.

Figure 2 shows representative ^{31}P spectra of unlabeled and $^{17}O/^{18}O$ double-labeled decamer. As can be seen in figure 2B/C, a decrease in intensity of a single resonance and a resonance with an associated upfield shifted peak is observed. Most of the resonances can clearly be distinguished, each integrating for one phosphorus resonance. Note that there are slight chemical shift changes of some of the resonances attributed to small differences in sample concentration, solvent, and temperature. The resonance of the ^{17}O-labeled phosphate is observed as a reduced intensity peak in figures 2B/C and the ^{18}O-labeled phosphorus resonance as an upfield shifted signal to the remaining unlabeled phosphate signal. (The $H_2^{17}O$ sample also contains both $H_2^{16}O$ and $H_2^{18}O$; see Experimental.) This can be seen in figures 2B and C where the ^{18}O-labeled phosphate ^{31}P signal is shifted slightly upfield relative to the remaining ^{16}O phosphorus resonance (37).

Table I. P-31 Chemical Shifts and P-H3′ Coupling Constants for Duplex (CCCGATCGGG)

Base	P-3l(ppm)[a]	18.5°C J(P-H3′) Hz	30°C J(P-H3′) Hz	50°C J(P-H3′) Hz	80°C J(P-H3′) Hz
C1					
p	–3.974	3.8	4.0	5.2	6.6
C2					
p	–3.974	3.8	5.0	5.2	6.6
C3					
p	–3.736	5.0	5.2	6.6	7.0
G4					
p	–4.066	5.8/2.6	5.8	5.2	6.6
A5					
p	–4.321	2.2	3.4	2.6	5.8
T6					
p	–4.199	2.6	3.2	4.0	5.8
C7					
p	–4.072	5.8/2.6	5.8	5.2	6.6
G8					
p	–3.709	5.0	5.2	5.0	6.2
G9					
p	–3.914	6.0	5.0	5.2	7.0
G10					

a. P-31 chemical shifts referenced to trimethyl phosphate (0.000 ppm).

The individual ^{31}P chemical shifts of the decamer duplex phosphorus signals (referenced to trimethyl phosphate, 0 ppm) are tabulated in table I and plotted vs. sequence in figure 4.

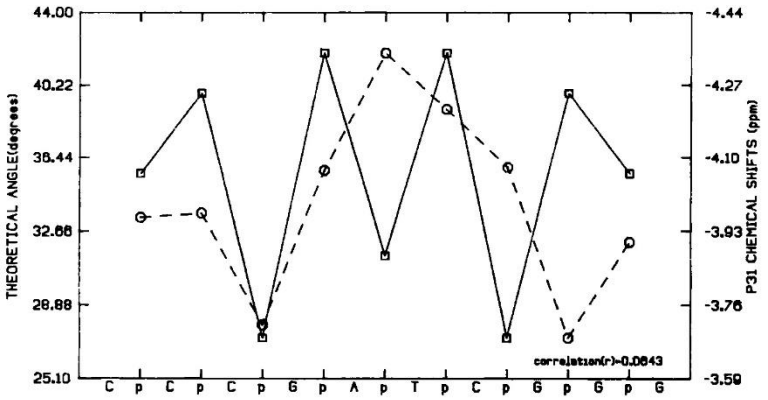

Figure 4. Plot of ^{31}P chemical shift (--O--) vs. phosphate position along the 5′-3′ strand for duplex decamer. Also shown is a plot of calculated helix twist sum, t_g, derived from calculated Σ_1 sum function and equation [1]{$t_g = 35.6 + 2.1\Sigma_1$) vs. phosphate position (--□--). The t_g vs. sequence plot has been scaled to reflect the ^{31}P chemical shift variations.

As shown in figure 4 (and better illustrated in figure 5) there exists a strong correlation between ^{31}P chemical shifts of complementary residues of the decamer. Figure 5 compares ^{31}P chemical shifts for complementary positions for the decamer duplex sequence, where the solid line connects ^{31}P chemical shifts for phosphate positions starting at the 5′ end and proceeding in the 3′ direction, and the dashed line represents ^{31}P chemical shifts for the complementary 3′-5′ strand.

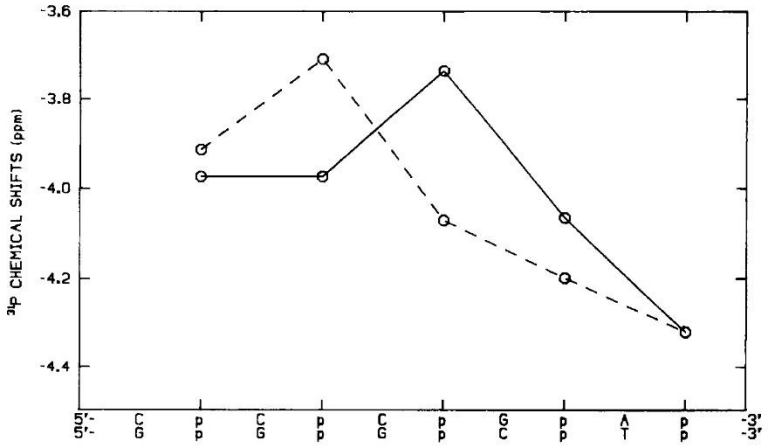

Figure 5. ^{31}P chemical shift pattern comparison of complementary phosphate positions of decamer. Solid lines: 5′-3′ direction; dashed lines: complementary 3′-5″ direction.

Note that because of the palindromic symmetry of the oligonucleotide, the corresponding phosphates on opposite strands that are related by the two-fold dyad axis of symmetry are chemically and hence magnetically equivalent. However, the "complementary" phosphates (phosphates opposite each other on complementary strands) are chemically and magnetically nonequivalent. As previously noted (63), the ^{31}P chemical shifts at complementary phosphate positions generally follow the same pattern in both strands of the duplex regardless of base sequence or position, suggesting that the phosphate geometry (see below) is nearly the same in complementary positions along both strands.

Positional and Sequence-Specific Variation of ^{31}P Chemical Shifts and Backbone Torsional Angles

As mentioned above, one factor that will affect ^{31}P chemical shifts is the degree of conformational constraint imposed by the duplex geometry (58,59,63,64). Note that the ^{31}P chemical shift of phosphates 3 through 8 (fig. 4) move upfield the more interior the phosphate. Base pairs closer to the ends of the duplex are less constrained to the stacked, base-paired geometry. This "fraying" at the ends imparts greater conformational flexibility to the deoxyribose phosphate backbone, and thus phosphates at the ends of the duplex will tend to adopt more of a mixture of g^-, g^- and t,g^- conformations. Interior phosphates are more constrained to the polymer P-O g^-, g^- conformation.

This "positional" ^{31}P chemical shift effect is apparently superimposed on a sequence-specific effect (12,15,58,59,63). The minor groove clash steps (pyrimidine-purine base steps) have been generally associated with a relatively downfield ^{31}P chemical shift. However as can be seen from the ^{31}P chemical shift pattern shown in figure 4, the minor groove clash steps at phosphate positions 3 and 7 appear to follow the positional effect. The relative upfield shift of phosphates 1, 2, and 9 are presumably attributed to the sequence-specific effect.

As discussed in more detail below, two of the most important parameters controlling ^{31}P chemical shifts in phosphate esters are the P-O torsional angles (in nucleic acids the P-O5′ (α) and P-O3′ (ζ) torsional angles (65,66) and the C-O5′ (β) and C-O3′ (ε) torsional angles) (67,68), although the P-O torsional angle may be more important. Using the selective 2D-J resolved long-range correlation experiment, we can measure the three-bond H3′-C3′-O-P coupling constant (listed in table I) for each of the phosphates in the decamer (48,63). The 2D spectra at selected temperatures are shown in figure 6.

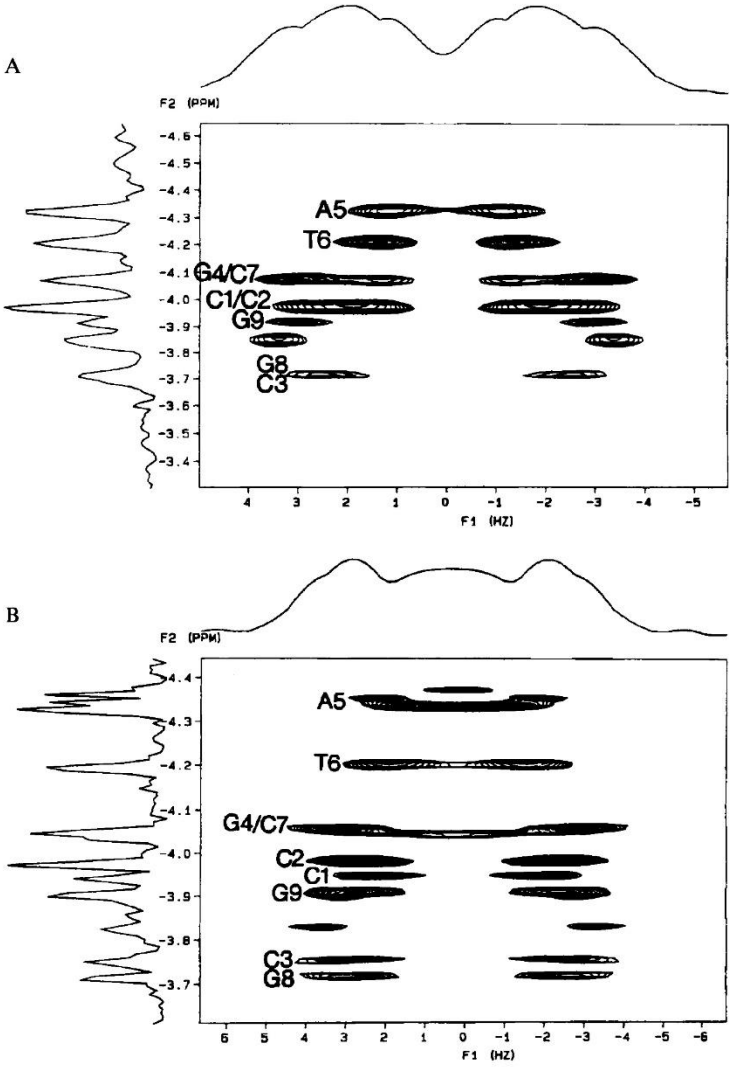

Figure 6. 2D-J resolved long-range correlation spectrum of decamer. The 1D decoupled ^{31}P NMR spectrum is also shown along one axis and the H3′ coupled doublets are shown along the second dimension (A) 18.5°, (B) 30°, (C) 50°, and (D) 80°.

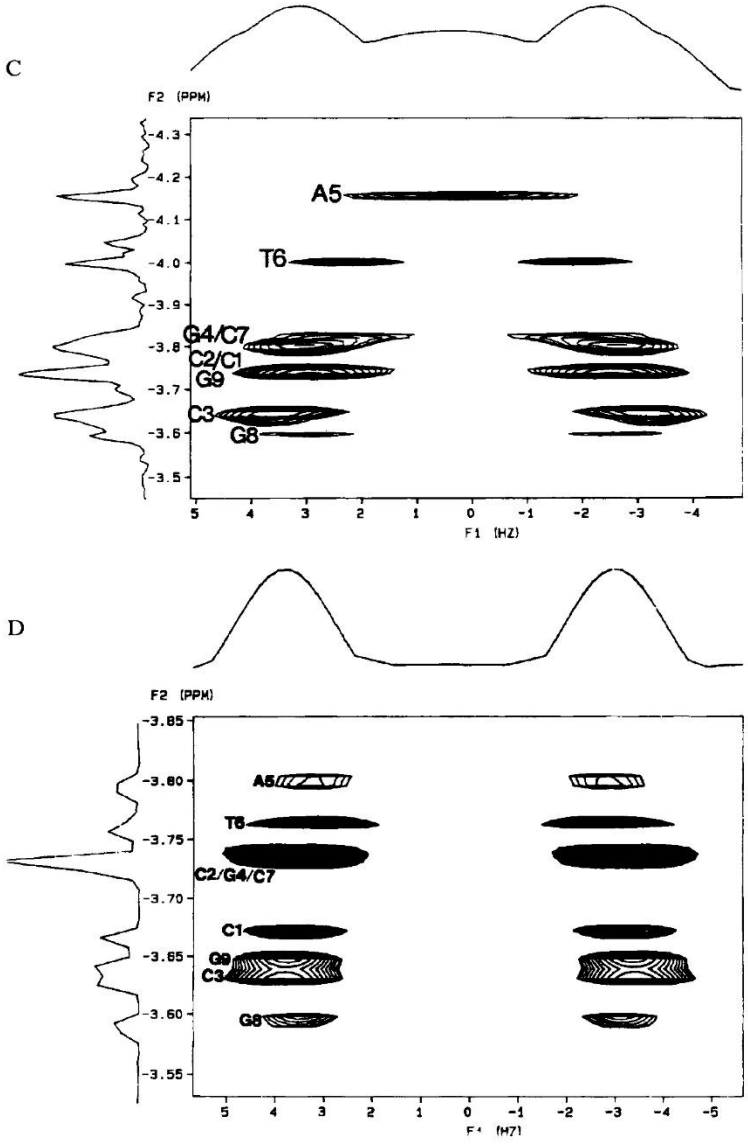

Figure 6, *continued*

Combined with a proton-phosphorus Karplus relationship (see Experimental Section) we can determine the H3′-C3′-O-P torsional angle θ from which we have calculated the C4′-C3′-O-P torsional angle ε. Up to four different torsional angles (0–360°) may be derived from the same coupling constant, and we assume that the torsional angle ε closest to the crystallographically observed value of ca. = –169° ± 25° (1) is the correct value. As shown by Dickerson (3,4) there is a strong correlation (R = –0.92) between torsional angles ζ and ε in the crystal structures of a dodecamer (ζ may be calculated from the relationship (3,4) ζ = –317 – 1.23ε). Thus, assuming this correlation of ζ and ε exists for other duplex structures in solution as well, and from the measured coupling constants, we can calculate both

C4′-C3′-O3′-P(ε) and C3′-O3′-P-05′ (ζ) torsional angles. A plot of the variation of both ζ (and ε) vs. ^{31}P chemical shifts for the decamer sequence is shown in figure 7.

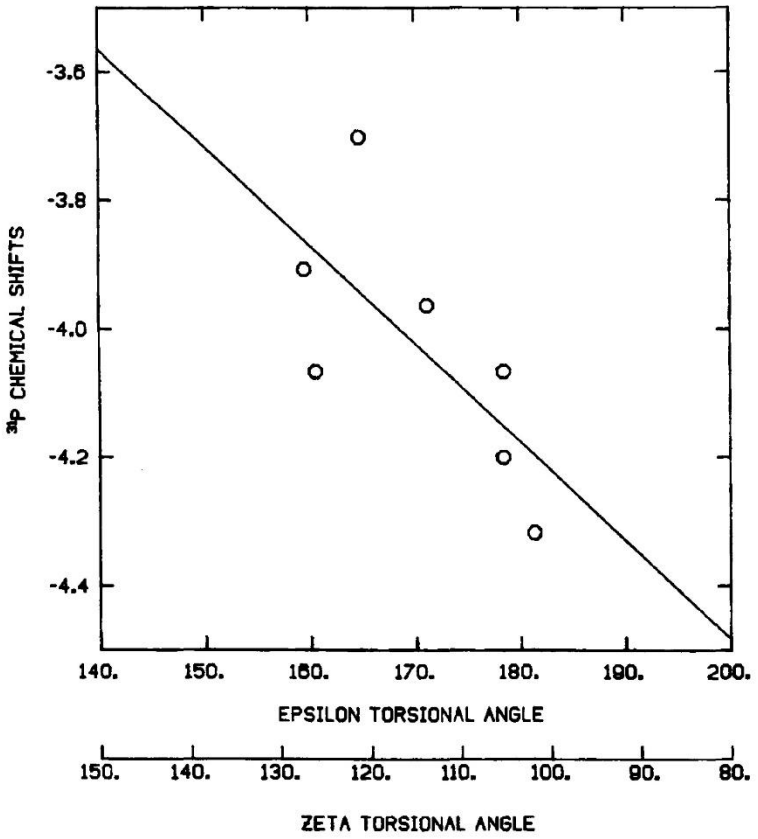

Figure 7. Comparison of ^{31}P chemical shifts and P-O3′ ester torsional angle ζ and C-O3′ torsional angle ε for the decamer (O). ζ torsional angle calculated from the $J_{H3'-P}$ coupling constants derived from figure 6, the calculated ε torsional angle from the Karplus relationship, and the correlation between ε and ζ (ζ = –317 – 1.23ε; note that there is a typographical error in the 96 paper).

The correlation coefficient between ζ (or ε) and ^{31}P chemical shifts varies from –0.69 (at ambient temperature) to –0.89 (at 50°C; the negative sign indicates that an increase in ε results in a decrease in the ^{31}P chemical shift). We have also confirmed that $J_{H3'-P}$ coupling constants and ^{31}P chemical shifts are strongly correlated for several other oligonucleotide duplexes (62,63).

The data of figure 7 supports our hypothesis that the positional-specific and sequence-specific variation in ^{31}P chemical shifts is largely attributable to variations in the helical parameters and the backbone torsional angles (at least for ζ and ε). Unwinding or winding the double helix changes the backbone α and ζ torsional angles, and these backbone

changes presumably are responsible for the variations in the ^{31}P chemical shifts of oligonucleotides.

The ^{31}P NMR spectrum of the [MeCys^3, MeCys^7]TANDEM · decamer complex is very similar to that of the decamer alone (spectrum not shown). Binding of an intercalating drug unwinds the duplex (1) and causes a downfield shift of the ^{31}P signal (64,69). This unwinding and lengthening of the deoxyribose phosphate backbone allows the drug to insert with a base-to-base separation of 6.7 Å to accommodate the intercalated drug. This is apparently accomplished by the phosphate switching from the normal B-DNA conformation ("B_I") in which both P-O torsional angles ζ and α are in the g^- conformation to the "B_{II}" conformation (ζ = t, $\alpha = g^-$). The ^{31}P signal of a phosphate in a t, g^- B_{II} conformation is predicted to be ~1–1.5 ppm downfield from the g^-, g^- phosphate in the B_I conformation (64,70), and we expect to observe a large downfield shift of the ^{31}P signal upon binding of a drug to DNA by intercalation. Note that *none* of the phosphates in the [MeCys^3, MeCys^7]TANDEM · decamer complex is shifted significantly downfield relative to the decamer phosphate signals. This is strong support for the binding of the drug to the duplex by a nonintercalative mechanism. The 2D-heteronuclear correlated and J resolved long-range correlation spectra of the [MeCys^3, MeCys^7]TANDEM · decamer duplex complex (fig. 8 and 9) demonstrate that binding of the drug produces some selective changes in the backbone torsional angles of the duplex. Note specifically the reduction in the ^{31}P-^1H three-bond coupling constant (from 5.4 to 2.0 Hz) of one of the most downfield of the ^{31}P signals.

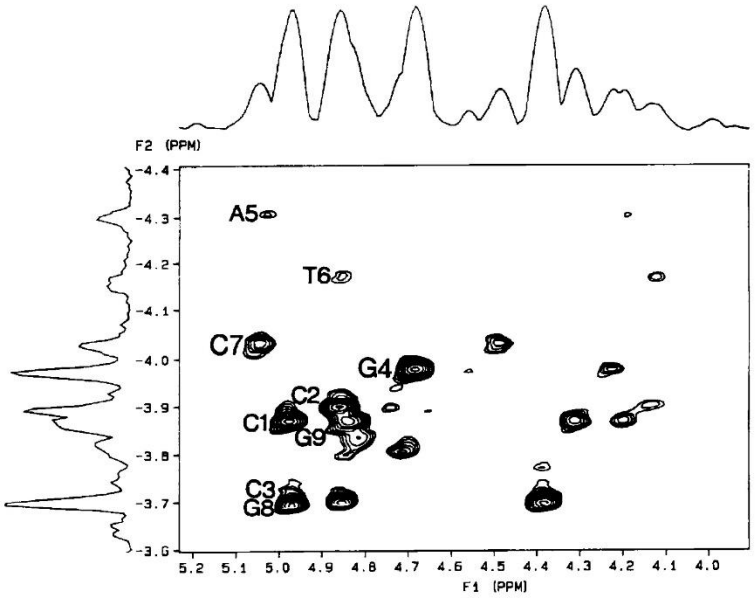

Figure 8. Two-dimensional ^{31}P-^1H PAC heteronuclear correlation NMR spectrum of [MeCys^3, MeCys^7]TANDEM · decamer duplex complex at 200 MHz (^1H). The 1D decoupled ^{31}P NMR spectrum is shown along one axis and the H3′, H4′, and H5′5″ region of the proton spectrum is shown along the second axis.

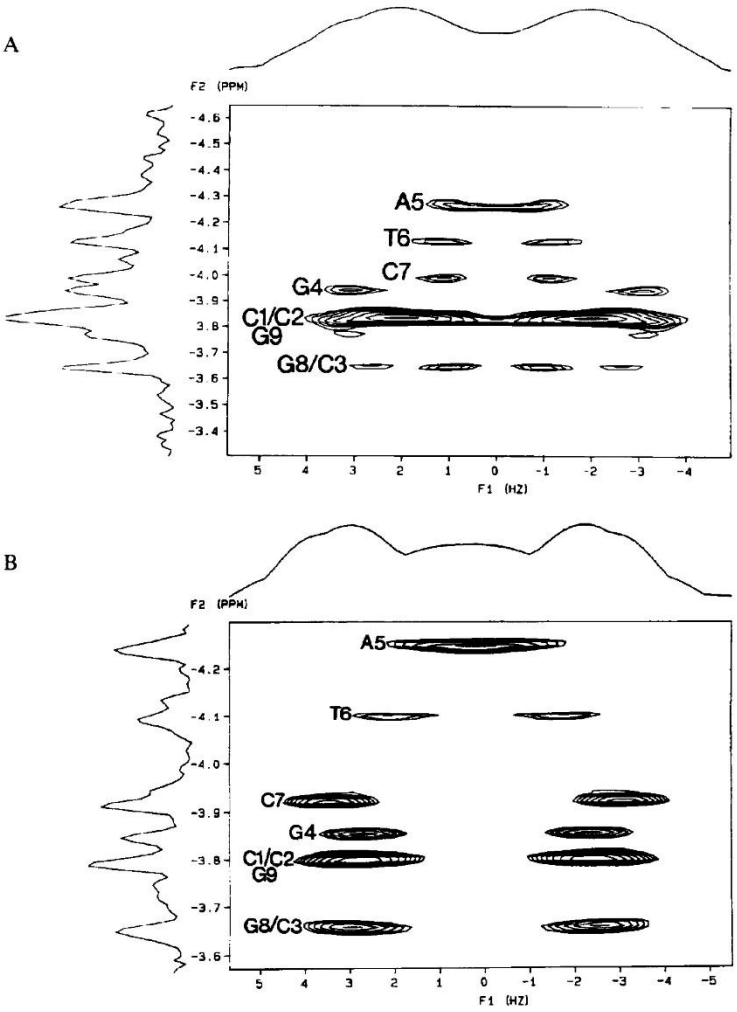

Figure 9. 2D-J resolved long-range correlation spectrum of [MeCys^3, MeCys^7]TANDEM · decamer duplex complex. The 1D decoupled ^{31}P NMR spectrum is also shown along one axis and the H3′ couplex doublets are shown along the second dimension. (A) 18.5°, (B) 30°, (C) 50°, and (D) 80°.

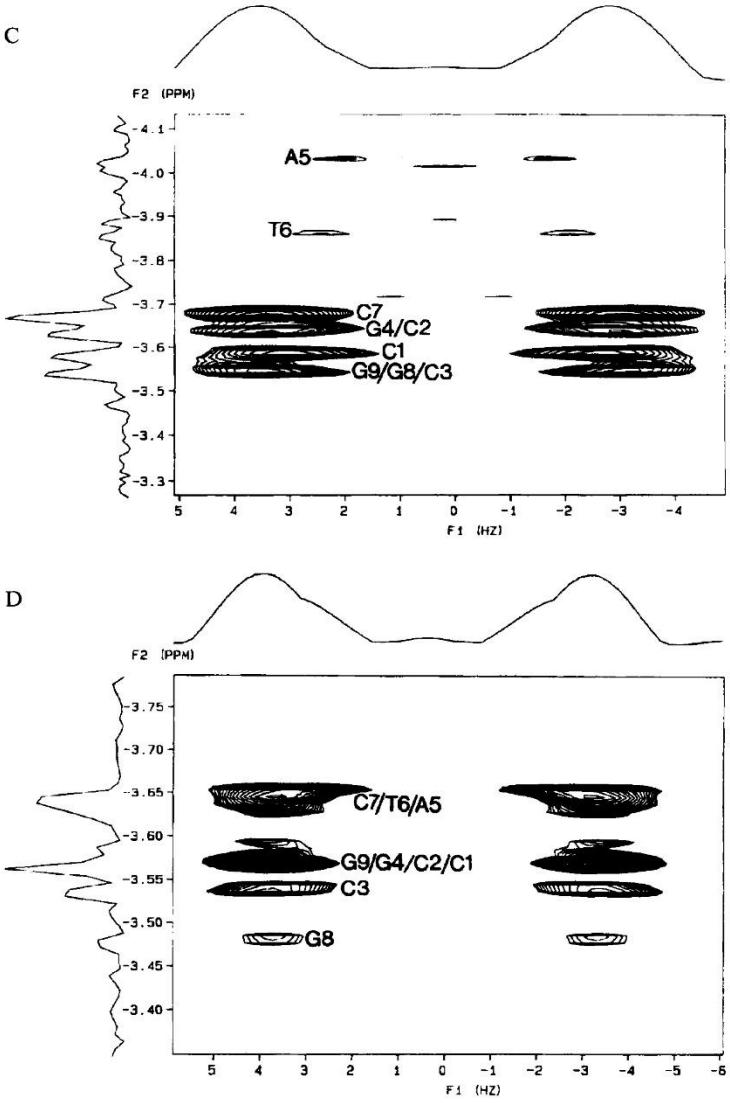

Figure 9, *continued*

Proton NMR of Decamer Duplex

The sequence-specific assignment methodology (9, 10,12–14, 16) was used to identify the proton NMR signals of the decamer. The two-dimensional NOESY and COSY spectra of DNA contain definitive regions of proton chemical shifts. These regions correspond to the aromatic base (H8/H6) region, the sugar H1′ and base H5 region, the sugar H2′/H2″ region and the sugar H3′, H4′ and H5′/H5″ region (see fig. 10 for the NOESY spectrum of the decamer duplex; the COSY spectrum is not shown—all spectra not shown are available upon request from the authors). In a typical B-DNA conformation, the distance between a sugar H1′ proton and its base proton and the (N-1) base proton to the 5′ end are within the ca. 5 Å NOE limit (71). Thus, the base proton's diagonal peak will have two corresponding

NOE crosspeaks, except for the 5′ end base which will have only an NOE to its own H1′ sugar proton. This allows for a sequential assignment of the H1′ sugar protons and the base protons down the DNA backbone. The usual starting point is at the 5′ end base since it has only one corresponding NOE crosspeak. The next base in the sequence will have an NOE which will line up with the 5′ end (N-1) base's lone NOE (H1′-H8/H6 inter-residue NOE) and its own H1′-H8/H6 intra-residue NOE. The sequential assignment continues down the DNA backbone through a series of inter and intra H1′-H8/H6 NOEs (fig. l0B).

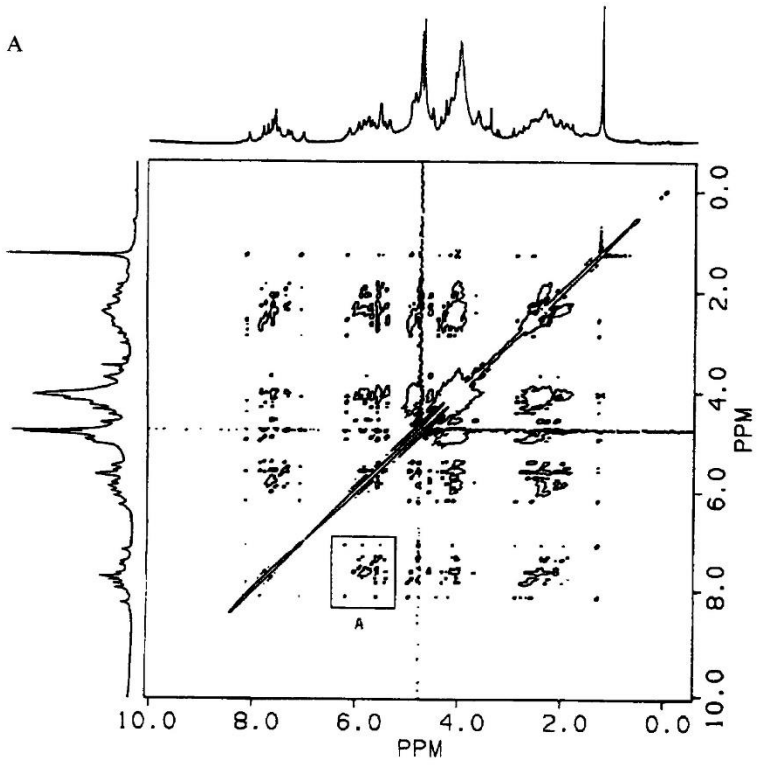

Figure 10. (A) Pure absorption phase $^{1}H/^{1}H$ NOESY NMR spectrum of duplex decamer, at 470 MHz. (B) Region labeled A is expanded in 10B. The sequential assignment of the base and deoxyribose H1′ protons is diagrammed.

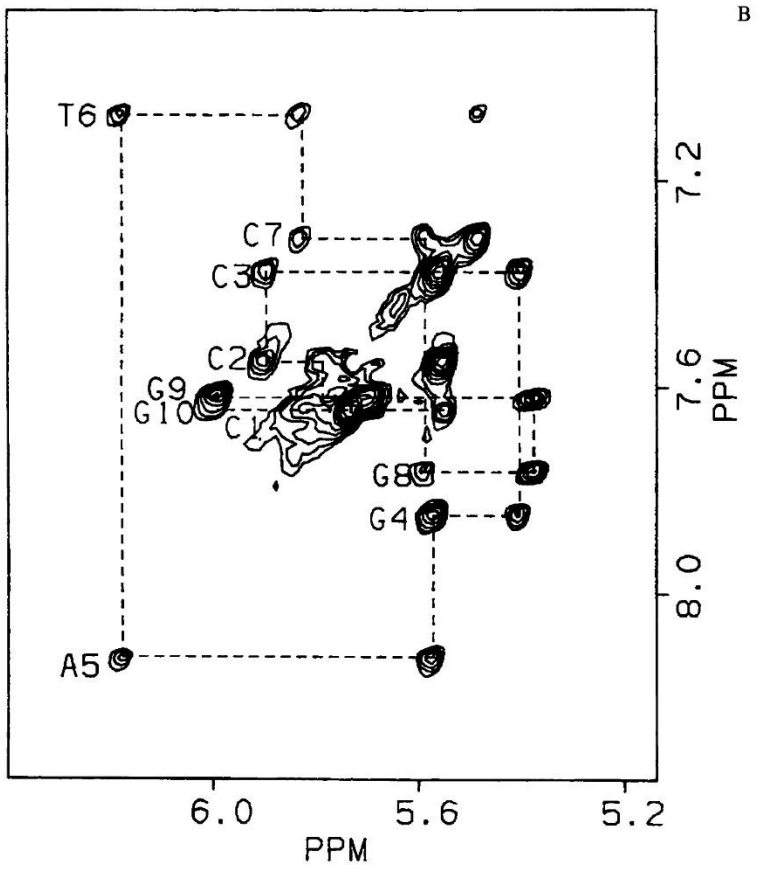

Figure 10. *continued*

Additional NOEs are seen, based on typical B-DNA structure, between H5 and H6, H1′ and H3′, H1′ and H2′/H2″, base protons and H2′/H2″, base protons and (N-1) H2′/H2″ to the 5′end, H4′ and H5′/H5″, H3′ and H4′, H2′and H2″. All the additional protons can be assigned after the H1′ and base protons have been assigned based on the previous list of NOE connectivities. These additional NOEs allow for a secondary path if ambiguities arise in the H1′ to H8/H6 sequential assignment or allow for redundancy in the assignments. The base to H2′/H2″ region contains four crosspeaks, except for the 5′-end base. The intra-residue base to H2′/H2″ crosspeaks can be identified by comparing them with the cross-peaks in the H1′ to H2′/H2″ region. Similar to the H1′ to base region, a sequential walk can be made down the DNA backbone from intra-base to H2′/H2″ NOEs to inter-base to H2′/H2″ NOEs. In essence, it is possible to walk around the entire NOESY spectrum to complete the assignments. Connectivities can be made from the Hl′ to H8/H6 region to the H8/H6 to H2′/H2″ region to the H1′ to H2′/H2″ region to the H1′ to H3′ region and back to the H1′ to H8/H6 region. This allows for redundancy checking and the presence of internal consistency.

This was the primary method of assigning the proton spectrum of the decamer. The major obstacle in assigning the decamer was the large overlap in the H1′ to base region (fig. l0B). The assignment of the 5′ end base by the presence of only one NOE was ambiguous. The sequential assignment began with the two highly resolved base resonances, one upfield and one downfield. The downfield resonance was assigned to A5 and the upfield resonance was assigned to T6. This was based on the normal distribution of chemical shifts of the base protons and the presence of a sequential connectivity between these two resonances. The remainder of the bases corresponded to either guanosine or cytosine. The cytosine base protons were assigned from the COSY spectrum (not shown). The COSY spectrum contains crosspeaks for the cytosine's J-coupled H5 and H6 protons. The COSY spectrum contains four crosspeaks in the base to H1′/H5 region corresponding to the four cytosines in the sequence. These same crosspeaks are observed as NOEs in the TPPI NOESY spectrum, which allows for the identification of the cytosine H6 protons and by default the guanosine H8 protons. The sequential assignments of the guanosines and the cytosines were then obtained by walking through the H1′ to base region starting from both the A5 resonance and proceeding in the 5′ direction and from the T6 resonance and proceeding in the 3′ direction. The assignments were verified by comparison to the base-H2′/H2″ NOE region connectivities and by following the path around the spectrum: base-H1′ NOE's to H1′-H2′/H2″ NOE's to base-H2′/H2″ NOEs and back to base-H1′ NOE's. The H3′, H4′, and H5′/H5″ protons were assigned from the direct NOE's between H1′-H3′ and from spin diffusion of the H1′ protons to H4′ and H5′/H5″ and from spin diffusion from the base protons to the H4′ and H5′/H5″ protons (observed in the NOESY spectra taken at long mixing times). The H3′, H4′, and H5′/H5″ protons are also distinguished by their relative chemical shifts in the order H3′ > H4′ > H5′/H5″.

As discussed above the PAC spectra (fig. 3) correlates the ^{31}P chemical shifts to the H3′, H4′, and H5′/H5″ proton chemical shifts through scalar coupling. Because some of the ^{31}P assignments were independently made by oxygen labeling of the phosphates (and hence some of the coupled protons could also be assigned) the PAC experiment provided confirmation of the NOESY ^{1}H assignments. The H5′ and H5″ protons were not stereospecifically assigned. The H2′/H2″ protons were stereospecifically assigned by their relative NOE intensity. In B-DNA, the H1′-H2′ crosspeak is always stronger than the H1′-H2″ crosspeak. The T6 methyl group was assigned from the thymidine H6 base proton to the methyl group COSY and NOESY crosspeaks. An additional NOESY crosspeak to the thymidine methyl group is seen from the A5 H8 base proton. The A5 H2 proton is assigned by default from the remaining peak in the aromatic region of the one dimensional proton spectrum. The proton chemical shifts of the decamer duplex are compiled in table II.

Table II. Proton Chemical Shift Assignments for Duplex

	PAC[a,b]/NOESY[a,c]								
Base	H6/H8	H5	H1′	H2′/H2″	H3′	H4′	H5′/H5″	CH3	H2
C1	7.64	5.73	5.79	2.08/2.42	4.89/4.90	4.54	4.11/4.01	—	—
C2	7.55	5.57	5.90	2.10/2.37	4.77/4.77	4.54	4.12/3.99	—	—
C3	7.38	5.57	5.40	1.96/2.30	4.77/4.76	—	4.20/4.03	—	—
G4	7.85	—	5.57	2.67/2.76	4.95/4:91	4.30	4.04/3.97	—	—
A5	8.12	—	6.18	2.56/2.87	4.93/4.94	4.40	4.18/4.09	—	7.69
T6	7.07	—	5.82	1.94/2.36	4.77/4.77	—	4.10/4.04	1.27	—
C7	7.31	5.59	5.59	1.85/2.24	4.95/4.95	4.55	4.15/4.03	—	—
G8	7.76	—	5.38	2.58/2.58	4.88/4.88	4.22	4.04/4.02	—	—
G9	7.62	—	5.99	2.39/2.27	4.76/4.89	4.30	4.11/4.04	—	—
G10	7.64	—	5.55	2.08/2.38	/4.90	4.54	4.11/4.01	—	—

a. Proton chemical shifts referenced to HDO at 4.76 ppm.
b. Chemical shifts assigned from the P-31/H-1 2D PAC spectrum.
c. Chemical shifts assigned from the H-1/H-1 NOESY spectrum.

The decamer-drug proton spectrum was assigned by comparing the two-dimensional TPPI NOESY spectrum of the decamer sample to the decamer · [MeCys[3], MeCys[7]]TANDEM spectrum (fig. 11).

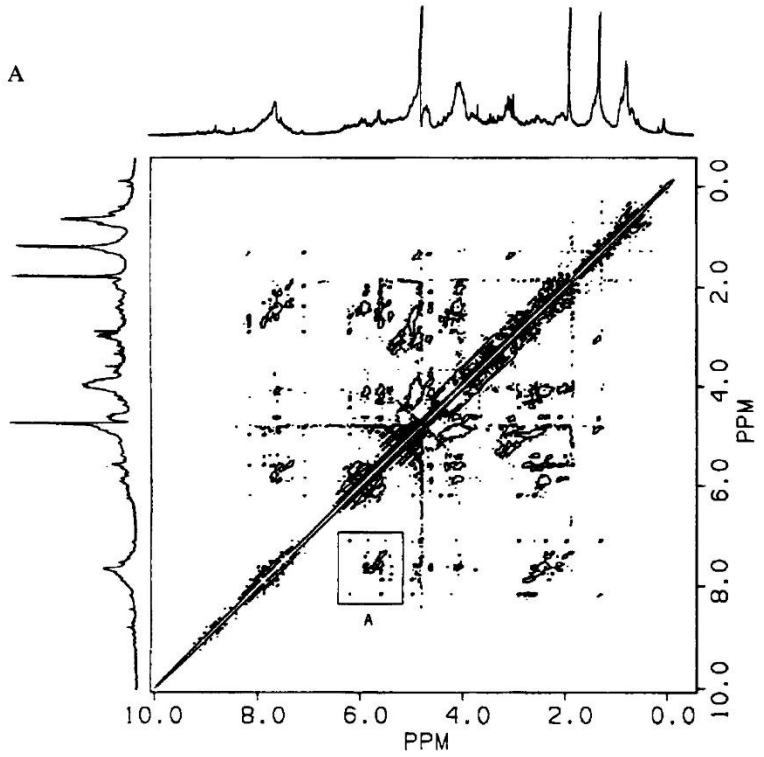

Figure 11. (A) Pure absorption phase ^{1}H-^{1}H NOESY NMR spectrum of duplex decamer · [MeCys^{3}, MeCys^{7})TANDEM complex (0.8:1), at 470 MHz. (B) Region labeled A is expanded in 11B. The sequential assignment of the base and deoxyribose H1′ protons is diagrammed.

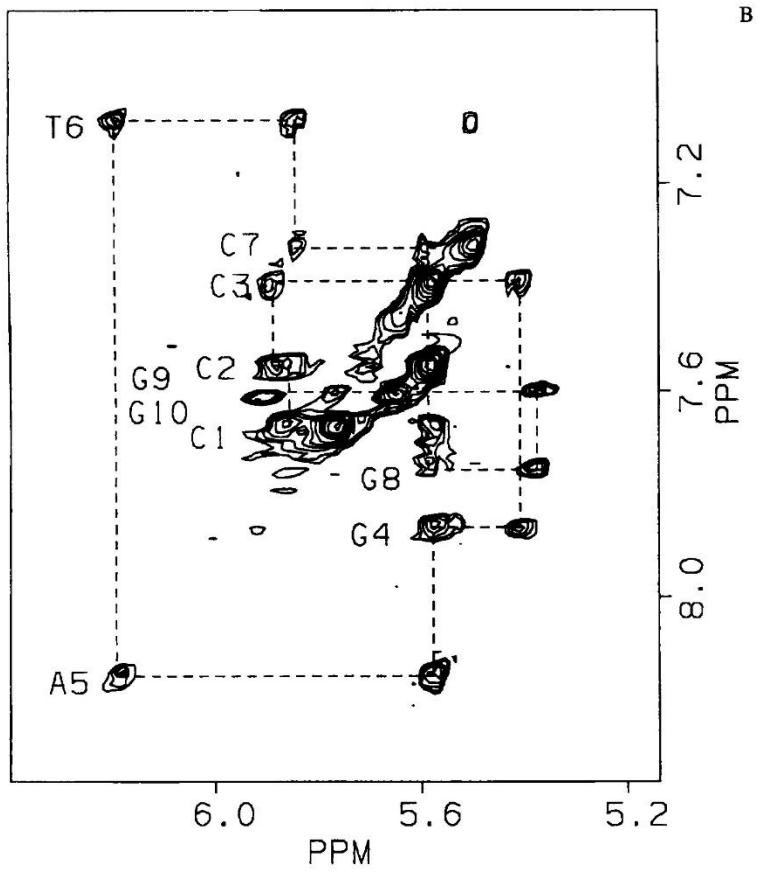

Figure 11, *continued*

The two spectra were basically identical. There were only minor chemical shift changes in the decamer-drug complex (on the average of ± 0.03 ppm) and no decamer to [MeCys^3, MeCys^7]TANDEM inter-residue NOEs were observed. [MeCys^3, MeCys^7]TANDEM intramolecular NOEs were observed between the C-alpha and C-beta protons of the cyclic depsipeptide. These crosspeaks overlapped greatly, and their assignment was not pursued further.

The assignment of the decamer's imino protons was based on relative chemical shifts and the melting profiles (69,72–75). There are ten imino protons in the sequence, but because of the palindromic nature of the sequence half of the protons are degenerate (fig. 12A).

The imino region of the decamer's proton spectrum (400 mM KCl) contained only three resonances. These resonances integrate (low to high field) for a ratio of 1:2:2 at 5°C. The imino protons of AT base pairs are invariably downfield from the imino protons of GC base pairs. Since the ratio of AT base pairs to GC base pairs in the decamer is one to four and the most downfield resonance integrates for one proton, the most downfield resonance was assigned to the AT base pair.

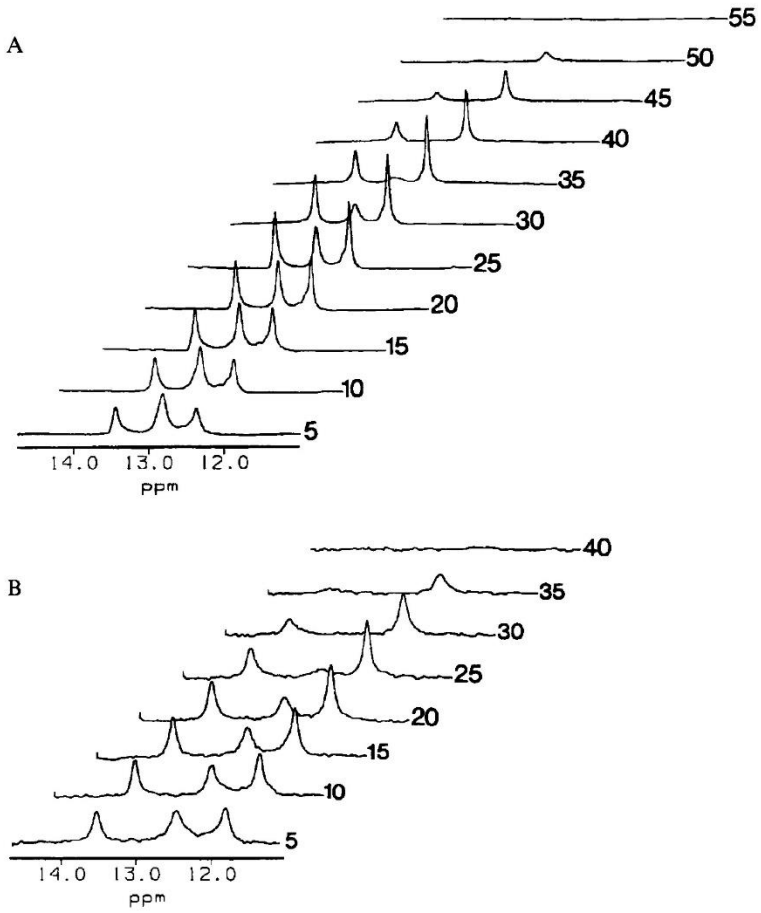

Figure 12. (A) Proton NMR spectrum of the imino proton region of the decamer duplex at indicated temperatures. (B) Proton NMR spectrum of the imino proton region of the decamer · [MeCys^3, MeCys^7)TANDEM complex at indicated temperatures.

It is possible to utilize the melting of the imino proton signals to discriminate between the interior and terminal base pairs. The imino protons are quite labile and exchange with water, resulting in a decrease in intensity and increase in linewidth of the imino proton resonance with temperature. An increase in the exchange rate of an imino proton is associated with transient breaking of the imino proton hydrogen bond and is generally reflective of a decrease in the stability of the base pair. The two remaining unassigned imino resonances are associated with the four GC base pairs and each resonance has a distinct melting temperature. The most up field resonance has a T_m of 25°C (fig. 12B). The remaining resonance has a T_m of 30°C. Because terminal base pairs generally melt (or undergo "fraying") at lower temperatures than interior base pairs—especially if the base pairs are of the same type—the most upfield resonance was assigned to the two terminal GC imino protons. By default, this leads the assignment of the middle imino resonance to the two internal GC base pairs.

Melting Curves

The UV melting curve of the decamer at low salt and DNA concentrations is shown in figure 13A. The ^{31}P chemical shift melting profile of the decamer is shown in figure 13B. The temperature dependence of the ^{31}P chemical shifts were followed by their relative position in the spectrum. It was assumed that no dramatic chemical shift changes occurred over the 5° intervals which could have resulted in relative positional exchange of any of the resonances.

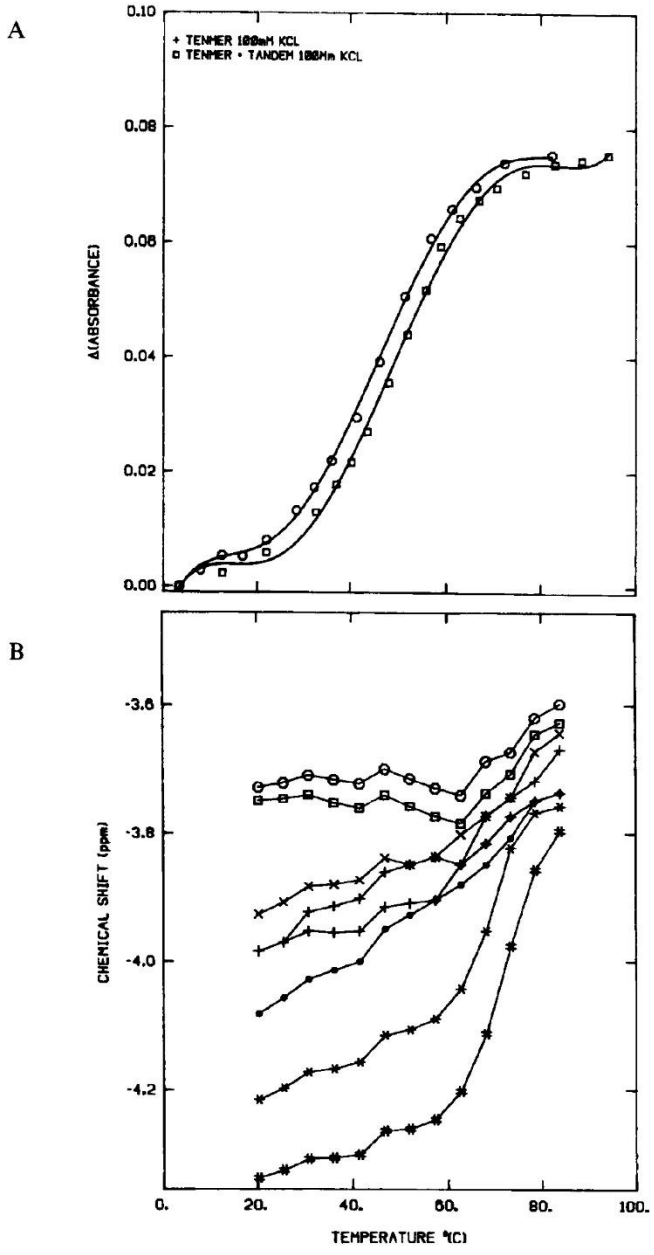

Figure 13, *continued on next page*

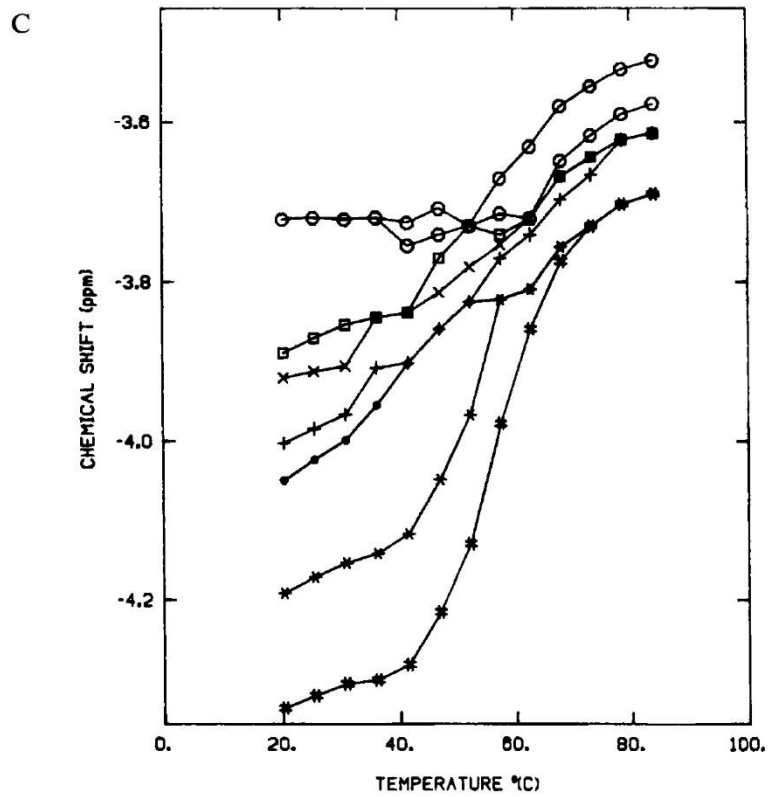

Figure 13. (A) Temperature dependence of UV absorbance at 260 nm of decamer (0) and decamer · [MeCys[3], MeCys[7]]TANDEM (0.8:1) complex (□) at 100 mM KCl. (B) Temperature dependence of the ^{31}P chemical shifts of the decamer. Phosphate positions 1 (+), 2 (+), 3 (□), 4 (O), 5 (#), 6 (*). 7 (O), 8 (O), and 9 (□). (C) Temperature dependence of ^{31}P chemical shifts of duplex decamer · [MeCys[3], MeCys[7]]TANDEM (0.8:1) complex. Phosphate positions 1 (X), 2 (X), 3 (O), 4 (+), 5 (#), 6 (*), 7 (O) and 8 (O) and 9 (D).

Drug · Duplex Complex

UV Titration

The decamer · [MeCys[3], MeCys[7]]TANDEM complex was titrated with 0.1 to 0.2 O.D. aliquots of decamer. The titration was monitored by UV spectroscopy either by observing the overall resulting spectrum after each aliquot addition or by a difference spectrum in which the initial spectrum was zeroed out and only the changes due to the aliquot additions were observed. The UV spectrum of the decamer · [MeCys[3], MeCys[7]]TANDEM complex showed a small change in the spectrum of the drug chromaphore, from which we have calculated via Scatchard analysis a binding constant, $K_a = 4.31 \times 10^4\ M^{-1}$ (r = 0.86).

^{1}HNMR Spectra of the Drug Complex

A TPPI COSY spectrum of the decamer · [MeCys[3], MeCys[7]]TANDEM complex provided improved resolution and the ability to observe the scalar coupling connectivities of the

peptide backbone in the complex. The cyclic depsipeptide segment of the drug is expected to be in a beta-sheet conformation from the known X-ray crystal structure of TANDEM. The beta-sheet structure of the cyclic depsipeptide is also expected from the presence of the disulfide crosslink which locks the two halves of the cyclic depsipeptide into antiparallel strands. The cyclic depsipeptide should give ^{1}H chemical shifts consistent with a beta sheet. The chemical shifts in a beta-sheet of the alpha protons are further downfield relative to the random-coil or alpha-helix. Typical alpha proton chemical shifts of valine, serine, cysteine, and alanine are centered about 4.5 ppm. The observed chemical shifts from the TPPI COSY of the decamer-drug complex are centered about 5.15 ppm. These results indicate that the cyclic depsipeptide portion of [MeCys^{3}, MeCys^{7}]TANDEM in the complex is in a beta-sheet structure. In addition, the alpha to beta proton region of the drug contained more cross peaks than expected. The proton NMR of the drug alone indicates that the amino acid residue protons of each Ala, Cys, Val, and Ser residues are degenerate due to the C2 axis of symmetry. The additional crosspeaks can be assigned to either slowly exchanging multiple conformations of the decamer drug complex or the protons are in magnetically distinct environments based upon the mode of binding. The presence of these additional crosspeaks suggests that the symmetry of the drug is lost upon binding to the decamer. However, there is no induced CD when the drug is bound to the decamer indicating that the symmetry of the drug is not disrupted upon binding to the decamer (Powers, unpublished). The lack of an induced CD is consistent with the absence of any drug-DNA NOEs and the relatively weak [MeCys^{3}, MeCys^{7}]TANDEM decamer complex binding constant. These results suggest a rapid exchange of the drug between free solution and a number of possible sites on the duplex.

Molecular Mechanics Energy Minimization Calculation of the Decamer and Decamer-TANDEM Complex

As described in the Experimental Section and in more detail below, structures for the decamer duplex and decamer-drug complex were derived from model building and energy minimization utilizing the AMBER program (51) and NOESY-distance constrained molecular mechanics calculations. The structures derived from these calculations are shown in figure 14.

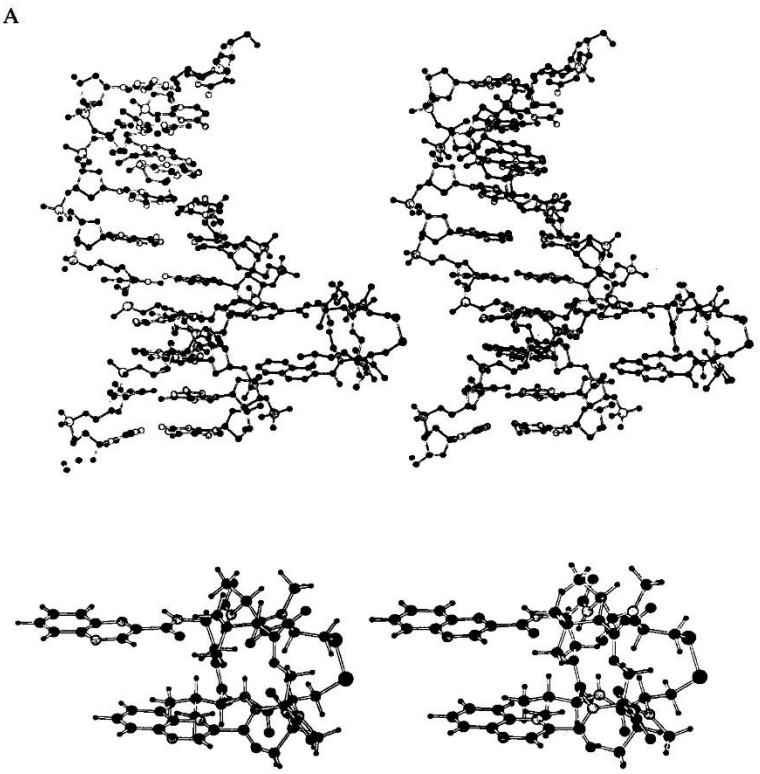

Figure 14. (A) NOESY-distance constrained, energy minimized structure of B-DNA built duplex decamer, d(CCCGATCGGG)$_2$ complexed with [MeCys^3, MeCys^7]TANDEM in the minor groove. The drug · decamer duplex complex was model build and energy minimized. (Stereo view of the drug alone is shown in the inset for clarity.) (B) van der Waals surface of drug illustrating the fit of the parallel quinoxaline rings fitting into the minor groove in A.

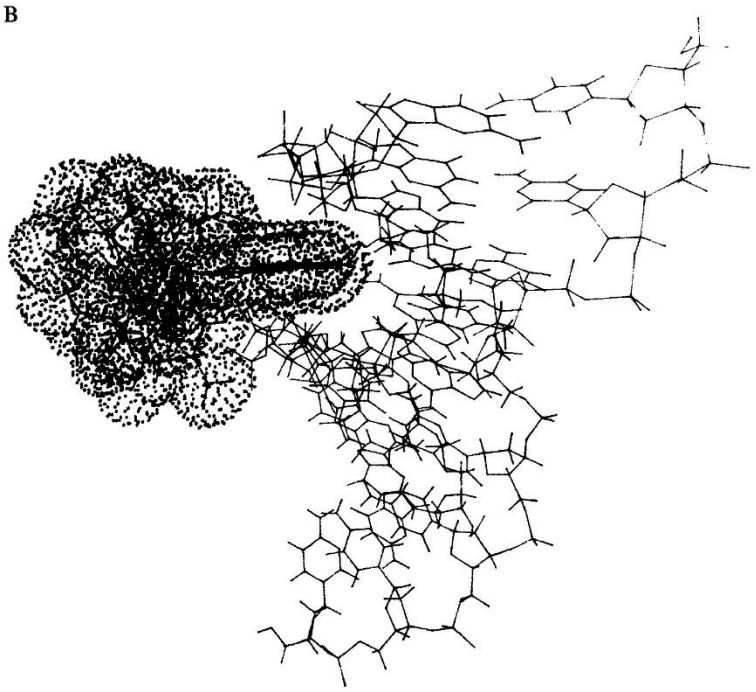

Figure 14, *continued*

Discussion

^{31}P Chemical Shifts as a Probe of DNA and DNA Drug Structure

We have noted that ^{31}P chemical shifts can potentially provide a probe of the conformation of the phosphate ester backbone in nucleic acids and nucleic acid complexes (60,64,76–79). These studies suggested that the ^{31}P resonance of a phosphate diester in a *g,g* or g^-,g^- conformation should be several ppm upfield of the ^{31}P signal of an ester in a *g,t* or *t,t* conformation (79).

If ^{31}P chemical shifts are sensitive to phosphate ester conformations, they potentially provide information on two of the most important torsional angles that define the nucleic acid deoxyribose phosphate backbone. One of these, the C3′-O3′-P-O5′ torsional angle, ζ, is also found to be the most variable one in the B-form of the double helix and the other O3′-P-O5′-C5′, α, torsional angle is one of the most variable in the A-form of the duplex (1). Indeed following the original suggestion of Sundaralingam (80) and based upon recent X-ray crystallographic studies of oligonucleotides, Saenger (1) has noted that the P-O bonds may be considered the "major pivots affecting polynucleotide structure."

With the recent development of methodologies to assign individual ^{31}P resonances of oligonucleotides (15,38,39,46,48,57,58,61,63,81) we have been able to begin to understand some of the factors apparently responsible for ^{31}P chemical shift variations in oligonucleotides (15,38,39,57,69,82–84). As discussed above, one of the major contributing factors that we have hypothesized determines ^{31}P chemical shifts is the main chain torsional angles of

the individual phosphodiester groups along the oligonucleotide double helix. Phosphates located toward the middle of a B-DNA double helix assume the lower energy, stereoelectronically (66) favored g^-,g^- conformation, while phosphodiester linkages located toward the two ends of the double helix tend to adopt a mixture of g^-,g^- and t,g^- conformations, where increased flexibility of the helix is more likely to occur. (The notation for the P-O ester torsion angles follows the convention of Seeman et al. (85) with the ζ, P-O-3′ angle given first followed by the α, P-O-5′ angle.) Because the g^-,g^- conformation is responsible for a more upfield ^{31}P chemical shift, while a t,g^- conformation is associated with a lower field chemical shift, internal phosphates in oligonucleotides would be expected to be upfield of those nearer the ends. Although several exceptions have been observed, this positional relationship appears to be generally valid for oligonucleotides where ^{31}P chemical shift assignments have been determined (12,15,57,58,60,86).

Eckstein and coworkers (57–59) and our laboratory (12,15,63) have recently suggested that ^{31}P chemical shifts are also sensitive to sequence-specific structural variations of the double helix as proposed by Calladine (2) and Dickerson (3). The ^{31}P chemical shifts of duplex B DNA phosphates correlate reasonably well with some aspects of the Dickerson/Calladine sum function for variation in the helical twist (or helical roll) of the individual base steps in the oligonucleotides. In the B-form DNA double helix with ~10 base pairs per turn (360°) of the helix each base pair is rotated ca. + 36° (helix twist) with respect to the nearest neighbor base pair. However, analysis (3) of X-ray crystallographic structures of a number of duplexes has revealed large variations in local helix structure, with helix twist varying from 25° to 45°. Correlations between experimentally measured P-O and C-O torsional angles and results from molecular mechanics energy minimization calculations show that these results are consistent with the hypothesis that sequence-specific variations in ^{31}P chemical shifts are attributable to sequence-specific changes in the deoxyribose phosphate backbone (63).

As shown in figure 4, ^{31}P chemical shifts of the central phosphates 3–8 of the duplex decamer appear to follow the positional relationship. *As* would be expected from the phosphate positional relationship, the ^{31}P chemical shifts in the central regions gradually increase (phosphates 3, 4, and 5), reach a maximum at the central phosphate position (5), and decrease once again for phosphates 6, 7, and 8.

However, in comparison to all other oligonucleotides studied (12,15,57–59,63), the ^{31}P chemical shifts of the decamer phosphates do not follow any of the predicted sequence-specific variations in either helix twist (R = –0.15) or roll angle (R = 0.38) based upon the Calladine rules. The CpG phosphate 3 is possibly shifted downfield relative to the expected value based upon the positional relationship. This is consistent with the expected pyrimidine-purine clash and unwinding at this base step (63). It is quite possible that chemical exchange of the duplex with other conformers (or even the hairpin loop state) is responsible for this lack of any significant sequence-specific ^{31}P chemical shift variations.

^{31}P NMR of Drug · DNA Complexes

^{31}P chemical shifts appear to be generally sensitive to changes in duplex structure resulting from binding of drugs to the duplex (73,78,82,87). Thus ^{31}P chemical shifts reflect differences in the unwinding angles in both DNA and RNA double helix-drug complexes (62,73,87,88). Insertion (intercalation) of a drug between the stacked base pairs reduces the helix twist of the duplex and the resulting decrease in the helix twist is termed the unwinding angle. Numerous mono-intercalating drugs produce an unwinding angle of 10–26°; the bis-intercalating drugs generally give unwinding angles twice that of the mono-intercalators (1). This unwinding of the DNA helix appears to produce changes in the P-O torsional angles (ζ, α) from a g^-,g^- to values such as t,g^- (1). Experimentally, downfield shifts on the order of 1.0 to 2.6 ppm are observed when drugs intercalate into DNA, reflecting these backbone torsional angle changes (78,82). The phosphorus resonances that shift downfield have been assigned to the phosphates which bridge the intercalated base pair (38,61).

The ^{31}P NMR spectrum of the decamer · [MeCys^3, MeCys^7]TANDEM complex is very similar to that of the decamer alone. There are no large downfield shifts upon addition of the drug. In fact, there are some modest upfield chemical shifts of a few of the phosphorus resonances, which is often observed in nonintercalative, groove binding of other drugs to duplex DNA (69,78). Correlating specific bases to the phosphorus resonance which are affected is not possible since the peaks correspond to degenerate phosphorus signals. These modest changes in the ^{31}P NMR spectrum of the decamer · [MeCys^3, MeCys^7]TANDEM complex thus support a nonspecific, nonintercalation mechanism for the binding of the drug to the duplex.

Binding of [MeCys^3, MeCys^7]TANDEM to Decamer

The footprinting studies of TANDEM and [MeCys^3, MeCys^7]TANDEM on a 160 base pair fragment from the *E. Coli* trp promoter sequence indicated that both drugs protect an average of seven base pairs of DNA (21,41,89). [MeCys^3, MeCys^7]TANDEM protects only two sites on the restriction fragment, centered about ApTpT or TpApT. Previous studies on the quinoxaline antibiotics indicate a bis-intercalation mode of association of the drug (36), suggesting a similar mechanism for [MeCys^3, MeCys^7]TANDEM.

The interaction between decamer and [MeCys^3, MeCys^7]TANDEM was initially established by the ability of the decamer to bring the drug into an aqueous buffer solution. The solubility of [MeCys^3, MeCys^7]TANDEM in an aqueous solution is only 6 μM. The decamer sample was capable of bringing it into solution at millimolar concentrations consistent with the measured binding constant of [MeCys^3, MeCys^7]TANDEM for the decamer (K_a = 4.31×10^4 M^{-1}).

The UV spectrum of the decamer · [MeCys^3, MeCys^7]TANDEM complex provided the initial indication that the drug was not intercalating into the decamer. The typical effect on the UV spectrum of an intercalating drug is a shift in the maxima to a longer wavelength and a decrease in the extinction coefficient (hypochromicity) (26,35). The maxima and extinction coefficient of the [MeCys^3, MeCys^7]TANDEM drug were perturbed by only a small degree upon binding to the decamer, suggesting that the decamer does not undergo any major conformational changes upon drug binding and that binding did not occur by bis-intercalation.

When mono-intercalators and bis-intercalators bind to DNA they induce major changes in the UV melting curves of DNA The quinoxalines increase the T_m of various DNA polymers by +l.0 to +8.5°C with drug/base pair ratios as low as 0.005 to 0.046 (35,90). The binding of [MeCys^3, MeCys^7]TANDEM to decamer induces a modest 2.5°C increase in the T_m of the decamer only at a high drug/base pair ratio of 0.1. This result indicates only a mild stabilization of the decamer helix implying that intercalation is not the mode of binding.

Structure of the decamer · [MeCys^3, MeCys^7]TANDEM complex

The lack of major perturbations in the UV, proton, and phosphorus NMR spectra of the [MeCys^3, MeCys^7]TANDEM · decamer complex, strongly supports a nonintercalative binding of the drug to the decamer. Because separate NMR resonances are not observed for the drug complex and the decamer alone, this interaction is fast on the NMR time scale. In addition, the lack of large site-specific perturbations in the NMR spectra suggest that the drug undergoes rapid chemical exchange between multiple, nonintercalative binding sites. While it is not possible to define a unique drug-duplex complex structure, the ^{31}P chemical shift melting profile (fig. 13B) of the decamer · [MeCys^3, MeCys^7]TANDEM complex provides some indication of possible regions of the drug-DNA contacts. In contrast to the overall increase in the UV melting temperature of the complex relative to the duplex alone of 2.5° (fig. 13A), the presence of the drug results in a decrease in the melting temperature of three of the phosphorus resonances. Thus the T_m of the phosphate corresponding to the peak at –4.321 ppm (A5pT6) decreases from 65°C to 50°C, the resonance at –4.199 ppm (T6C7) decreases from 60°C to 45°C and the resonance at –3.709 ppm (G8pG9) decreases from 65°C to 55°C. These sites of local destabilization suggest specific regions of contact between [MeCys^3, MeCys^7]TANDEM and the decamer sugar phosphate backbone (compare fig. 13B and C).

Additional points of DNA-drug contacts may be inferred from the temperature dependence to the imino spectra and the imino proton chemical shift melting profile (fig. 12). Analogous to the ^{31}P melting profile, the binding of the drug has *decreased* the stability of some of the base pairs as monitored by the T_m of the imino protons. The GC base pairs were destabilized more than the AT base pair. The melting temperature of the terminal and internal GC imino protons in the duplex decreases from 30°C to 20°C and from 45°C to 35°C, respectively in the drug complex. It could be argued that these imino and phosphorus signal effects could be attributable to the residual amount of acetonitrile that remains in solution despite repeated efforts for its removal by relyophilization of the sample. However, we believe that these *selective* decreases in the melting temperatures of several residues as monitored by ^{1}H NMR of the imino protons and ^{31}P NMR of the backbone phosphates are real effects representing some degree of sequence specificity in the binding of the drug to the duplex. Note that overall, the melting temperature, as monitored by UV spectral changes show that the drug stabilizes the duplex form relative to the random coil, denatured form. Because ^{1}H and ^{31}P NMR are run at 1000-fold higher concentrations than the UV spectra, and because NMR monitors different melting phenomena, it is not proper to attempt to directly compare the different measures of melting temperatures.

Additional information establishing some specific interaction of the drug with the second phosphorus from the end comes from the 2D ^{31}P-^{1}H long-range J-resolved spectra (fig.

6 and 9). The ^{31}P-H3′ coupling constant of either the phosphorus resonance at –3.709 ppm (G8pG9) or –3.736(C3pG4) decreases from 5.4 Hz to 2.2 Hz upon addition of [MeCys^{3}, MeCys^{7}]TANDEM (overlap of the signals prevents definitive assignments). This change in coupling constant implies a decrease from 175° to 150° in the C4′-C3′-O-P torsional angle.

Molecular Modeling of Decamer Duplex

Using the distances derived from the 2D NOESY spectrum of figure 10, in conjunction with restrained molecular mechanics and dynamics calculations, we derived a structure for the duplex decamer. Distances were calculated by integrating the crosspeaks and utilizing the two-spin approximation at short mixing times (71). Although volumes were measured for a complete set of mixing times (50, 100, 200, 300, 400, 500, and 700 ms) the volumes for a single 200 ms TPPI NOESY were used to measure the intra and inter proton distances from the observed NOE crosspeaks (table III).

The NOESY buildup curves (data not shown) demonstrated that the NOEs were primary NOEs not appreciably affected by spin diffusion. (A complete relaxation matrix calculation analysis of the NOESY buildup curves has confirmed that the qualitative features of the structures described are essentially correct. A comparison of the structures derived from both the two-spin approximation at various mixing times and a complete relaxation matrix (91) approach will be described in Meadows et al., in preparation.) Starting from an idealized model-built duplex structure, we have used NOESY-derived distances to constrain the molecular mechanics/dynamics energy minimization program AMBER (51) to minimize the energy of the decamer duplex. Instead of a simple harmonic potential error function to restrain the NMR-derived distances, we have modified AMBER so as to provide a flat well harmonic function which better reflects the intrinsic accuracy of these NOESY distance restraints (62,92). We have generally used an estimated error of ± 15% in the NOESY distances.

Table III. NOE Distances Derived from 200 msec NOESY Spectrum of Duplex

Intranucleotide Distances (R_{ij})[a]							
Base	H6/H8 to H1′	H6/H8 to H2′	H6/H8 to H2″	H6/H8 to H3′	H1′ to H2′	H1′ to H2″	H1′ to H3′
C1	—	—	—	—	2.51	2.18	—
C2	2.80	2.23	2.58	—	2.63	2.37	2.55
C3	3.26	2.53	2.61	—	2.64	2.41	—
G4	2.77	2.20	2.31	2.79	2.52	2.45	2.66
A5	3.25	2.65	2.74	2.83	2.68	2.57	3.25
T6	3.34	2.75	2.86	—	2.61	2.36	—
C7	—	2.63	2.76	—	2.64	2.39	—
G8	2.86	—	—	3.19	—	—	2.76
G9	—	2.54	—	—	2.25	2.22	—
G10	3.18	—	—	—	2.46	2.27	—

Internucleotide Distances ($R_{i,j-1}$)[a]			
Base	H6/H8 to H1′	H6/H8 to H2′	H6/H8 to H2″
C1	—	—	—
C2	—	—	—
C3	3.20	—	2.91
G4	3.20	3.35	2.74
A5	2.75	3.26	2.79
T6	3.26	3.44	2.88
C7	3.28	—	—
G8	3.28	3.36	2.48
G9	2.75	—	—
G10	—	—	—

a. All distances referenced to C7 (H5/H6) crosspeak, assuming a reference distance of 2.45 angstroms.

While some differences are observed between the constrained and unconstrained minimized duplexes (particularly at the ends of the duplex where fraying of the strands is possible), the main features of the B-DNA duplex are retained in both the dynamics and mechanics calculations.

Molecular Modeling of [MeCys³, MeCys⁷]TANDEM · Duplex Complex

The results from the imino proton chemical shift melting curve, ^{31}P melting curve and the 2D ^{31}P-^{1}H long-range J-resolved spectrum of the drug duplex complex indicate possible points of contact between the drug and the second and fifth phosphate along the DNA backbone. The AMBER program was used to calculate an energy minimized structure for the decamer · [MeCys³, MeCys⁷]TANDEM complex. Thus the initial decamer part of the drug complex structure was based upon the distances derived from the free duplex NOESY spectra and the distance-constrained, minimized structure. The binding of the [MeCys³, MeCys⁷]TANDEM to the decamer resulted in significant increases in the ^{1}H NMR linewidths. A significant amount of resolution enhancement was required to analyze the decamer · drug complex NOESY spectrum, which precludes accurate integration of the NOESY crosspeak volumes. However, as shown in figure 11A/B, the drug complex spectra

are qualitatively similar to the duplex spectra (fig. l0A/B), indicating little overall perturbation in the B-DNA geometry. An energy-minimized structure of [MeCys^3, MeCys^7]TANDEM, based upon the X-ray structure of TANDEM, was docked onto the decamer using the molecular modeling program MIDAS. The [MeCys^3, MeCys^7]TANDEM drug was positioned at one end of the decamer in the minor. Although the crystal structure of the Triostin A · d(CGTACG)$_2$ complex shows that the cyclic peptide linking the bis-intercalated quinoxaline rings binds in the minor groove, the quinoxaline heterocycles of these drugs are physically too large to fit into the minor groove without intercalation or rotation about the serine-quinoxaline bonds. However, simple rotation about the serine-quinoxaline C(O)-aromatic ring bonds moves the quinoxaline rings from a self-stacking conformation to a coplanar orientation which allows the quinoxaline rings to easily insert deeply into the minor groove (fig. 14A/B). In the minor-groove structure, only the two quinoxaline rings can be easily inserted deep within the groove without major deformation of the duplex structure (fig. 14B). The walls of the minor groove are quite hydrophobic and the tight fit of the aromatic chromophores provides a significant amount of the interaction energy between the drug and duplex. The side chain of the two valines also approaches just to the van der Waals radii of the hydrophobic side of the sugar residues, providing further stabilization of the complex. Note that the depsipeptide is on the outside of the groove.

Most interestingly, this minor-groove binding geometry places the nonintercalating quinoxaline rings at an ca. 45° angle relative to the stacked base pairs. It appears quite reasonable to envision a process whereby the quinoxaline ring rotates so that the chromophore is now co-planar to the base-pairs (requiring some opening also of the minor groove), and with unwinding of the duplex the chromophore can now easily intercalate between the stacked base pairs. This would be the mono-intercalated geometry and further twisting and intercalation of the other quinoxaline ring, followed by the depsipeptide ring settling into the widened minor groove would complete the bis-intercalation process. We therefore suggest that the minor-groove structure could represent the initial encounter complex with the DNA, not only for the bis-intercalators but possibly as well for mono-intercalators such as Actinomycin D.

Groove Binding vs. Bis-lntercalation

Because we do not observe any drug to duplex NOE crosspeaks, the drug must bind in a nonspecific mode. All of our observations point to a nonintercalative mode of association of the [MeCys^3, MeCys^7]TANDEM to the duplex decamer. However, previous studies have suggested that this drug, and others related to it, binds to DNA via a mixture of mono-intercalation and bis-intercalation with multiple binding sites. Nonspecific surface (or groove) binding have been postulated only as an intermediate in the exchange between different binding modes and binding sites. The primary factors that influence the ability of the quinoxaline and related drugs to bis-intercalate are the nature of the linker between the chromophores as well as the DNA sequence. A minimum length of 10 Å is required to allow the two chromophores to bis-intercalate about a "sandwiched" base pair so as not to violate the nearest-neighbor exclusion principle. A stiff linker is also required to prevent self-stacking of the chromophores in an aqueous environment (20,21). Self-stacking has been observed for some of these bis-intercalators (23).

The [MeCys^3, MeCys^7]TANDEM meets all of the criteria required for a good bis-intercalator. The quinoxaline class of antitumor drugs have been shown to be bis-intercalators (17,25–27,35). This includes the quinomycin drug echinomycin and the triostin drugs—triostin A and its derivative TANDEM. Based upon proton NMR and X-ray crystallography the various quinoxaline drugs have the same basic C-shaped structure with the quinoxaline rings planar to each other and perpendicular to the rectangular shaped cyclic depsipeptide (28–30,31).

The heterogeneity in the binding modes has also been monitored by the effect of the binding constants under varied conditions. The bis-intercalators show a dramatic increase in DNA affinity and binding constants relative to mono-intercalators. Mono-intercalators have binding constants on the order of 10^5 M^{-1}; binding constants are affected by drug concentration, ionic strength, and temperature. As the concentration of drug to duplex is increased, all the bis-intercalators experience an increase in the relative amount of bis-intercalation and a decrease in the amount of mono-intercalation and nonspecific binding. The points of these transitions are drug dependent but usually occur at an r value (defined as the ratio of drug bound to DNA base pairs) of 0.2 for bis-intercalation and an r value of 0.1 for mono-intercalation (18,20). The bis-intercalators stabilize the DNA to a greater extent (higher T_m) in a solution of low ionic strength, which implies a higher percentage of bis-intercalation. Higher temperature favors mono-intercalation over bis-intercalation, which implies that bis-intercalation is driven by the thermodynamics of chromophore stacking and mono-intercalation is driven by the properties of the depsipeptide-DNA interaction (93).

Ethidium bromide, a known intercalator, has been shown to have a secondary electrostatic binding site. This secondary binding site has a lower ligand binding affinity but can be populated at the expense of the primary binding mode. Competition between the primary and secondary binding sites is salt and buffer dependent. At high free-ligand concentration, the secondary binding site is the predominate mode of binding. The postulation of an intermediate nonspecific type of binding is supported by some of the work done with bis-intercalator derivatives. Some of these derivatives have linkers which are too short to allow for bis-intercalation or are methylated in a fashion to sterically hinder intercalation, resulting in compounds which are mono-intercalators or nonintercalators.

DNA binding constants for triostin A and TANDEM are on the order of 10^6 M^{-1} and 10^4 M^{-1}, respectively. The binding constants for the three quinoxaline drugs are dependent on the nature of the bound DNA. Both echinomycin and triostin A show a higher preference for DNA rich in GC, triostin greater than echinomycin. Gao and Patel (24) have shown that echinomycin appears to insert the quinoxaline rings between the A_1-C_2 and G_3-T_4 base steps in d $(ACGT)_2$, consistent with this specificity. However, TANDEM has a binding constant 1500 times greater when bound to AT-rich regions as compared to GC-rich regions. The [MeCys^3, MeCys^7]TANDEM also shows a binding site preference centered around ATA or TAT regions. The smaller binding constant to d(CCCGATCGGG)($K_a = 4.31 \times 10^4$ M^{-1}) is consistent with nonintercalative binding, and thus the AT base step in our sequence apparently does not provide an effective enough bis-intercalation site for binding the (MeCys^3, MeCys^7]TANDEM.

Conclusion

All of the evidence provided here support binding of the (MeCys[3], MeCys[7]TANDEM to a small DNA fragment possessing the correct specificity in a nonspecific minor groove binding mode. All previous evidence regarding these quinoxaline drugs such as [MeCys[3], MeCys[7]TANDEM has shown that the major interaction with DNA is either bis-intercalation or mono-intercalation. Most DNA-binding drugs that bind in a nonintercalative mode associate with the DNA through the narrow, minor groove and are significantly stabilized by hydrophobic interactions between the drug and the walls and floor of the minor groove (cf. netropsin and distamycin; 94,95). Although our model for the structure of the [MeCys[3], MeCys[7]TANDEM · decamer complex (fig. 14) is speculative and based largely upon the few ^{1}H and ^{31}P NMR perturbations induced by the drug, as well as model building and AMBER energy minimization, it represents a structure that, to our knowledge, is quite novel. In drugs such as netropsin and distamycin, the "thin edge" of the molecules (roughly the 3.4 Å thickness of an aromatic ring) appear to possess the appropriate crescent shape and dimensions to nicely insert into the helical narrow minor groove of the duplex (which varies from ca. 4–6 Å; 94,95). This fit of the natural crescent shape of the these drugs to the natural curvature of the DNA is probably at least partially responsible for their tight binding and sequence specificity (hence the preference for many of these drugs for the narrower minor groove in AT-rich regions of DNA). We have shown that the quinoxaline "bis-intercalators" are relatively constrained by the depsipeptide linkage so that the C-shape of the tethered quinoxaline rings prevents the thin edge of the drug from conveniently fitting into the minor groove without significant distortion of the drug. Perhaps as described in our model only the quinoxaline chromophores are deeply bound within the minor groove. This may represent the initial association complex which then is capable of forming the ultimate bis-intercalation complex in those sequences providing the appropriate interactions with the depsipeptide moiety.

Acknowledgments – Supported by NIH (GM36281 and AI27744), the Purdue University Biochemical Magnetic Resonance Laboratory which is supported by NIH (grant RR01077 from the Biotechnology Resources Program of the Division of Research Resources), the NSF National Biological Facilities Center on Biomolecular NMR, Structure, and Design at Purdue (grants BBS 8614177 and 8714258 from the Division of Biological Instrumentation) and the National AIDS Research Center at Purdue (AI727713). We greatly appreciate the contributions of Dr. Robert Santini, Dr. Claude Jones, Dr. Julian Tirado-Rives, and James Metz.

References and Footnotes

1. W. Saenger, *Principles of Nucleic Acid Structure*, Springer-Verlag, New York (1984).
2. C. R. Calladine, *J. Mol. Biol. 161*, 343–352 (1982).
3. R. E. Dickerson, *J. Mol. Biol. 166*, 419–441 (1983).
4. R. E. Dickerson and H. R. Drew, *J. Mol. Biol. 149*, 761–786 (1981).
5. J. A McClarin, C. A. Frederick, B. C. Wang. P. Greene, H. W. Boyer, J. Grable, and J. M. Rosenberg, *Science 234*, 1526–1541 (1986).

6. A. Hochschild and M. Ptashne, *Cell 44*, 681 (1986).
7. D. R. Kearns, *Crit. Rev. Biochem. 15*, 237–290 (1984).
8. T. L. James, *Phosphorus-31 NMR: Principles and Applications* (D. Gorenstein, ed.), 349–400, Academic Press, Orlando, 1984.
9. D. R. Hare, D. E. Wemmer, S. H. Chou, G. Drobny, and B. Reid, *J. Mol. Biol. 171*, 319 (1983).
10. J. Feigon, W. Leupin, W. A. Denny, and D. R. Kearns, *Biochemistry 22*, 5930–5942; 5943–5951 (1983).
11. D. Frechet, D. M. Cheng, L.-S. Kan, and P. O. P. Ts'o, *Biochemistry 22*, 5194–5200 (1983).
12. S. Schroeder, J. Fu, C. Jones, and D. G. Gorenstein, *Biochemistry 26*, 3812–3821 (1987).
13. M. A. Broido, G. Zon, and T. L. James, *Biochem. Biophys. Res. Commun. 119*, 663–670 (1984).
14. R. M. Scheek, R. Boelens, N. Russo, J. H. van Boom, and R. Kaptein, *Biochemistry 23*, 1371–1376 (1984).
15. S. Schroeder, C. Jones, J. Fu, and D. G. Gorenstein, *Bull. Magn. Reson. 8*, 137–146 (1986).
16. D. G. Gorenstein, R. P. Meadows, J. T. Metz, E. Nikonowicz, and C. B. Post, *Advances in Biophysics* in press (1989).
17. K. R. Fox, D. Gauvreau, D. C. Goodwin, and M. J. Waring, *Biochemistry J. 191*, 729–742 (1980).
18. R. G. Wright, P. G. Wakelin, A. Fieldes, R. M. Acheson, and M. J. Waring, *Biochemistry 19*, 5825–5836 (1980).
19. N. Assa-Munt, W. Leupin, W. A. Denny, and D. R. Kearns, *Biochemistry 24*, 1441–1449 (1985).
20. B. Gaugain, J. Barbet, N. Capelle, B. P. Roques, and J.-B. Le Pecq, *Biohemistry 17(24)*, 5078–5088 (1978).
21. J. W. Lown, B. C. Gunn, R. Y. Chang, K. C. Majumdar, and J. S. Lee, *Can. J. Biochem. 56*, 1006–1015 (1978).
22. A. Delbarre, M. I. Gourevitch, B. Gaugain, J. B. Le Pecq, and B. P. Roques, *Nucleic Acids Research 11*, 4467–4482 (1983).
23. D. M. Delepierre, B. L. D'Estaintot, J. Igolen, and B. P. Roques, *Biopolymers 26*, 1001–1033 (1987).
24. X. Gao and D. Patel, *Biochemistry 27*, 1744–1751 (1988).
25. R. H. Shafer and M. J. Waring, *Biopolymers 19*, 431–443 (1980).
26. J. S. Lee and M. J. Waring, *Biochem. J. 173*, 129–144 (1978).
27. J. S. Lee and M. J. Waring, *Biochem. J. 173*, 115–128 (1978).
28. M. A. Viswamitra, O. Kennard, W. B. T. Cruse, E. Egert, G. M. Sheldrick, P. G. Jones, M. J. Waring, and L. P. G. Wakelin, *Nature 289*, 817–819 (1981).
29. M. B. Hossain, D. van der Helm, R. K. Olsen, P. G. Jones, G. M. Sheldrick, E. Egert, O. Kennard, and M. J. Waring, *J. Am. Chem. Soc. 104*, 3401–3408 (1982).
30. E. Hyde, J. R. Kalman, D. H. Williams, D. G. Reid, and R. K. Olsen, *J. Chem. Soc., Perkin Trans I*, 1041–1048 (1982).
31. H. T. Cheung, J. Feeney, G. C. K. Roberts, D. H. Williams, G. Ughetto, and M. J. Waring. *Biopolymers 100*, 46–54 (1978).
32. B. F. Cain, B. C. Baguley, and W. A. Denny, *J. Med. Chem. 21(7)*, 658–668 (1978).
33. D. Pelaprat, A. Delbarre, I. Le Guen, and B. P. Roques, *J. Med. Chem. 23*, 1336–1343 (1980).
34. P. B. Dervan and M. M. Becker, *J. Am. Chem. Soc. 100*, 1968–1970 (1978).
35. M. J. Waring, L. P. G. Wakelin, and J. S. Lee, *Biochim. Biophys. 407*, 200–212 (1975).

36. A. H.-J. Wang, G. Ughetto, G. J. Quigley, T. Hakoshima, G. A. van der Marel, J. H. van Boom, and A. Rich, *Science 225*, 1115–1121 (1984).
37. D. O. Shah, K. Lai, and D. G. Gorenstein, *J. Am. Chem. Soc. 106*, 4302 (1984).
38. D. O. Shah, K. Lai, and D. G. Gorenstein, *Biochemistry 23*, 6717–6723 (1984).
39. K. Lai, D. O. Shah, E. Derose, and D. G. Gorenstein, *Biochem. Biophys. Res. Commun. 121*, 1021 (1984).
40. T. G. Lawson, F. E. Regnier, and H. L. Weith, *Analyt. Biochemistry 133*, 85–93 (1983).
41. C. M. L. Low, K. R. Fox, R. K. Olsen, and M. J. Waring, *Nucl. Acids Res. 14*, 2015–2032 (1986).
42. R. K. Olsen, K. Ramasamy, K. L. Bhat, C. M. L. Low, and M. J. Waring, *J Am. Chem. Soc. 108*, 6032–6036 (1986).
43. V. Sklenar and A. Bax, *J. Mag. Reson. 74*, 469–479 (1987).
44. D. Marion and K. Wuthrich, *Biochem. Biophys. Res. Comm. 113*, 967–974 (1983).
45. H. Kessler, C. Griesinger, J. Zarbock, and H. R. Loosli, *J. Magn. Reson. 57*, 331–336 (1984).
46. J. M. Fu, S. A. Schroeder, C. R. Jones, R. Santini, and D. G. Gorenstein, *J Magn. Reson. 77*, 577–582 (1988).
47. C. R. Jones, S. A. Schroeder, and D. G. Gorenstein, *J Magn. Reson. 80*, 370–374 (1988).
48. V. Sklenar and A. Bax, *J. Am. Chem. Soc. 109*, 7525–7526 (1987).
49. P. P. Lankhorst, C. A. G. Haasnoot, C. Erkelens, and C. Altona, *J. Biomol. Structure and Dynm. 1*, 1387–1405 (1984).
50. D. G. Gorenstein, E. M. Goldfield, R. Chen, K. Kovar, and B. A. Luxon, *Biochemistry 20*, 2141–2150 (1981).
51. P. K. Weiner and P. A. Kollman, *J. Comp. Chem. 2*, 287–303 (1981).
52. S. Arnott and D. W. L. Hukins, *J. Mol. Biol. 81*, 93–105 (1973).
53. M. J. S. Dewar, E. G. Zoebisch, F. H. Eamonn, and J. J. P. Stewart, *J. Am. Chem. Soc. 107*, 3902–3909 (1985).
54. T. E. Ferrin and Langridge, *Computer Graphics 13*, 320 (1980).
55. V. Sklenar, H. Miyashiro, G. Zon, H. T. Miles, and A. Bax, *FEBS Letters 208*, 94–98 (1986).
56. A. Pardi, R. Walker, H. Rapoport, G. Wider, and K. Wuthrich, *J. Am. Chem. Soc. 105*, 1652 (1983).
57. J. Ott and F. Eckstein, *Nucleic Acids Res. 13*, 6317–6330 (1985).
58. J. Ott and F. Eckstein, *Biochemistry 24*, 253 (1985).
59. B. A. Connolly and F. Eckstein, *Biochemistry 23*, 5523–5527 (1984).
60. D. G. Gorenstein, *Jerusalem Symposium, NMR in Molecular Biology* (B. Pullman, ed.), 1–15, D. Reidel Publishing Co. (1978).
61. M. Petersheim, S. Mehdi, and J. A. Gerlt, *J. Am. Chem. Soc. 106*, 439–440 (1984).
62. D. G. Gorenstein, C. R. Jones, S. A. Schroeder, J. T. Metz, J. M. Fu, V. A. Roongta, R. Powers, and C. Karslake, *Progress in Inorganic Biochemistry and Biophysics* (H. Gray and I. Bertini, eds.), Birkhauser, Inc., Boston, in press (1989).
63. D. G. Gorenstein, S. A. Schroeder, J. M. Fu, J. T. Metz, V. A. Roongta, and C. R. Jones, *Biochemistry 27*, 7223–7237 (1988).
64. D. G. Gorenstein, *Annual Review of Biophysics and Bioengineering 10*, 355 (1981).
65. D. G. Gorenstein and D. Kar, *Biochem. Biophys. Res. Commun. 65*, 1073–1080 (1975).
66. D. G. Gorenstein, *Chem. Rev. 87*, 1047–1077 (1987).
67. F. Ribas-Prado, C. Giessner-Prettre, B. Pullman, and J.-P. Daudey, *J. Am. Chem. Soc. 101*, 1737 (1979).

68. C. Giessner-Prettre, B. Pullman, F. Ribas-Prado, D. M. Cheng, V. Iuorno, and P. O. P. Ts'o, *Biopolymers 23*, 377 (1984).
69. D. J. Patel, *Accts. of Chem. Res. 12*, 118–125 (1979).
70. G. J. Quigley, A. H.-J. Wang, G. Ughetto, G. van der Marel, J. H. van Boom, and A, Rich, *Proc. Natl. Acad. Sci. USA* 77, 7204–7208 (1980).
71. K. Wuthrich, *NMR of Proteins and Nucleic Acids*, Wiley, New York, NY (1986).
72. D. J. Patel, *Biopolymers 15*, 533–558 (1976).
73. S. Chandrasekaran, R. L. Jones, and W. D. Wilson, *Biopolymers 24*, 1963–1979 (1985).
74. C. Giessner-Prettre and B. Pullman, *J Theoretical Biology 27*, 87–95 (1970).
75. D. J. Patel, S. A. Kozlowski, L. A. Marky, C. Broka, J. A. Rice, K. Itakura, and K. J. Breslauer, *Biochemistry 21*, 428–436 (1982).
76. D. G. Gorenstein and J. B. Findlay, *Biochem. Biophys. Res. Commun. 72*, 640 (1976).
77. D. G. Gorenstein, S. A. Schroeder, M. Miyasaki, J. M. Fu, V. Roongta, P. Abuaf, A. Chang, and J. C. Yang, *Biophosphates and Their Analogues-Synthesis, Structure, Metabolism and Activity* (K. S. Bruzik and W. J. Stec, eds.), 487–502, Elsevier Press, Amsterdam (1987).
78. D. G. Gorenstein and E. M. Goldfield, *Phosphorus-31 NMR:·Principles and Applications* (D. G. Gorenstein, ed.), Academic Press, New York (1984).
79. D. G. Gorenstein, *Phosphorus-31 NMR: Principles and Applications* (D. G. Gorenstein, ed.), Academic Press, New York (1984).
80. M. Sundaralingam, *Biopolymers* 7, 821–860 (1969).
81. D. G. Gorenstein, S. Schroeder, M. Miyasaki, J. Fu, C. Jones, V. Roongta, and P. Abuaf, *Proceedings of the 10th International Conference on Phosphorus Chemistry 30*, 567–570 (1987).
82. D. J. Patel, *Biochemistry* 13, 2396–2402 (1974).
83. D. M. Cheng, L.-S. Kan, P. S. Miller, E. E. Leutzinger, and P.O.P. Ts'o, *Biopolymers 21*, 697 (1982).
84. D. M. Cheng, L. Kan, and P.O.P. Ts'o, *Phosphorus NMR in Biology* (C. T. Burt, ed.), 135–147, CRC Press, Inc., Boca Raton (1987).
85. N. C. Seeman, J. M. Rosenberg, F. L. Suddath, J. J. Park Kim, and A Rich, *J. Mol. Biol. 104*, 142–143 (1976).
86. D. G. Gorenstein, J. B. Findlay, R. K. Momii, B. A. Luxon, and D. Kar, *Biochemistry 15*, 3796–3803 (1976).
87. R. L. Jones and W. D. Wilson,.*J. Am. Chem. Soc. 102*, 7776–7778 (1980).
88. K. Lai and D. G. Gorenstein, *Biochemistry 28*, 2804–2812 (1989).
89. C. M. Low, R. K. Olsen, and M. J. Waring, *FEBS Letters 176*, 414–420 (1984).
90. R. C. Thompson, *Methods Enzymol. 46*, 220–225 (1977).
91. J. Keepers and T. James, *J. Magn. Reson. 57*, 404 (1984).
92. G. M. Clore, A. M. Gronenborn, A. T. Brunger, and M. Karplus, *J. Mol. Biol. 186*, 435–455 (1985).
93. E. S. Canellakis, Y. H. Shaw, W. E. Hanners, and R. A. Schwartz, *Biochim. et Biophys. Acta 418*, 277–289 (1976).
94. M. Coli, C. A. Frederick, A. H. Wang, and A. Rich, *Proc. Natl. Acad. Sci. USA* 84, 8385–8689 (1987).
95. C. Zimmer and U. Wahnert, *J. Mol. Biol. 47*, 31–112 (1986).
96. A. V. Fratini, M. L. Kopka, H. R. Drew, and R. E. Dickerson, *J. Biol. Chem. 257*, 14686–14707 (1982).